COMPARING THE ECONOMIC PERFORMANCE OF ICE STORAGE AND BATTERIES FOR BUILDINGS WITH ON-SITE PV THROUGH MODEL PREDICTIVE CONTROL

A Dissertation

Submitted to the Faculty

of

Purdue University

by

Kairui Hao

In Partial Fulfillment of the

Requirements for the Degree

of

Master of Science in Mechanical Engineering

May 2020

Purdue University

West Lafayette, Indiana

THE PURDUE UNIVERSITY GRADUATE SCHOOL
STATEMENT OF DISSERTATION APPROVAL

Dr. James E. Braun, Chair

School of Mechanical Engineering

Dr. Donghun Kim

School of Mechanical Engineering

Dr. Ilias Bilionis

School of Mechanical Engineering

Approved by:

Dr. Nicole Key

Head of the School Graduate Program

ACKNOWLEDGMENTS

First and foremost, I am grateful to my major advisors Prof. Braun and Dr. Kim, who gave me the opportunity to work in Ray W. Herrick Laboratories for pursuing my Masters degree. The past two-year period for me was an unforgettable personal and educational experience that I couldn't imagine before. My research couldn't have been completed without your immense knowledge and patient guidance. Besides, you also inspired me in how to always stay passionate through my life.

I greatly appreciate all the staff and my colleagues in Ray W. Herrick Laboratories for creating such a fantastic and special research hub every single day. Because of all your work, my life and research experience were never monotonous.

TABLE OF CONTENTS

Page

Page

LIST OF TABLES

LIST OF FIGURES

Figure Page

SYMBOLS

$C_{p,w}$	specific heat of water/glycol mixture fluid
C^i_{PV}	installed cost per PV panel
C^m_{PV}	annual maintenance fee per PV panel
C^i_{ba}	battery installed cost per unit of energy storage capacity
C^m_{ba}	battery annual maintenance cost per unit of energy storage capacity
C_s	total ice storage capacity
C_b	battery energy storage capacity
C_r	battery C-rate
CWL	building cooling load
D	demand charge rate
DP	pressure differentials
E	time of use energy rate
I	battery charging and discharging current
M	plant modes
$\dot{m}_s$	mass flow rate passing two ice storage tanks
$\dot{m}_{s,0}$	mass flow rate passing two ice storage tanks at test conditions
$\dot{m}_{CH,i}$	chiller inlet mass flow rate
$\dot{m}_{CH}$	mass flow rate passing chiller
$\dot{m}_{CHWR}$	mass flow rate from buildings
n	number of PV panels
N_e	number of 15-minute time intervals
N_d	number of hourly time intervals
N_y	number of hourly time intervals in one year

N_m	number of months
N_s	number of ice tanks
P_{tb}^{15}	15-minute average total building electrical load
P_{tb}^{60}	60-minute average total building electrical load
P_b	battery charging and discharging power
P_{pump}	pump power
P_{CH}	chiller plant power
P_g	net hourly average power purchased from grid
P_l	hourly average building electricity load
P_g	net hourly average power purchased from grid
P_s	total hourly average PV power generation rate
P_{si}	single PV panel power
P_w	present worth factor
Q_{CH}	chiller cooling capacity
Q_{CHL}	chiller cooling load to meet $T_{CHe,SP}$
$Q_{CH,max}$	maximum chiller cooling capacity
Q_{BL}	building cooling load
Q_{ISL}	ice storage cooling load to meet $T_{CHWS,SP}$
$Q_{IS,max}$	maximum ice storage capacity
$Q_{IS,CR}$	ice storage charing rate
Q_{IS}	ice storage charging and discharging rates
$Q_{bat,I}$	battery current capacity
Q_{bat}	battery energy capacity
SC_{PV}	Present Value of system costs
T_{OA}	outdoor dry bulb temperature
$T_{CHe,SP}$	chiller exit temperature setpoint
$T_{CHWS,SP}$	primary chilled water supply temperature setpoint
$T_{CH,i}$	chiller inlet temperature
$T_{CH,e}$	chiller exit temperature

$T_{s,i}$	ice storage inlet temperature
$T_{s,e}$	ice storage outlet temperature
T_{CHWR}	return water temperature from building
T_{fr}	freezing point temperature
ΔT	time step
u	specific internal energy of the water and ice mixture
u_f	internal energy of saturated liquid water
u_{sf}	latent heat of fusion for ice
x_s	ice storage state of charge
x_b	battery state of charge
Δt	dicretized time step
$\epsilon_{C,0}$	ice storage charging heat transfer effectiveness for the test flow rate
$\epsilon_{D,0}$	ice storage discharging heat transfer effectiveness for the test flow rate
ϵ_C	ice storage charging heat transfer effectiveness
ϵ_D	ice storage discharging heat transfer effectiveness
η_{pump}	pump efficiency
η_{motor}	motor efficiency
$\eta_{inveter}$	inverter efficiency

ABSTRACT

Hao Kairui MSME, Purdue University, May 2020. Comparing the Economic Performance of Ice Storage and Batteries for Buildings with On-site PV through Model Predictive Control. Major Professor: James E. Braun.

Integrating renewable energy and energy storage systems provides a way of operating the electrical grid system more energy efficiently and stably. Thermal storage and batteries are the most common devices for integration. One approach to integrating thermal storage on site is to use ice in combination with the cooling system. The use of ice storage can enable a change in the time variation of electrical usage for cooling in response to variations in PV availability, utility prices, and cooling requirements. A number of studies can be found in the literature that address optimal operation of on-site PV systems with batteries or ice storage. However, although it is a natural and practical question, it is not clear which integrated storage system performs better in terms of overall economics. Ice storage has low initial and maintenance costs, but there is an efficiency penalty for charging of storage and it can only shift electrical loads associated with building cooling requirements. A battery's round-trip efficiency, on the other hand, is quite consistent and batteries can be used to shift both HVAC and non-HVAC loads. However, batteries have greater initial costs and a significantly shorter life. This research presents a tool and provides a case study for comparing life-cycle economics of battery and ice storage systems for a commercial building that has chillers for cooling and an on-site photovoltaic system. A model predictive control algorithm was developed and implemented in simulation for the two systems in order to compare optimal costs. The effect of ice storage and battery sizing were studied in order to determine the best storage sizes from an economic perspective and to provide a fair comparison.

1. INTRODUCTION

This chapter is aimed at providing research problem statements and background descriptions for the thesis. Several previous studies are reviewed and their contributions and limitations are addressed. Objectives and uniqueness of this study are presented.

1.1 Overview of developments of energy storage systems and photovoltaic technology

The building sector has been the largest consumer of energy in the world over the past decades. Consequently, the utilization of on-site renewable energy resources combined with energy storage is seen as a powerful approach for mitigating energy consumption and accommodating demand response (DR). In order to induce end-users to manage their energy consumption behaviors wisely for the purpose of demand response, numerous utility companies offer time-dependent utility rate structures, which discourage on-peak electricity usage by employing time-of-use (TOU) energy cost rates and demand charges. Additionally, net energy metering (NEM) [1] as a renewable energy resources policy, which allows self-generated energy fed back into the grid with the same retailing price, further incentivizes on-site distributed energy resource devices. Among all kinds of renewable energy technologies, installed photovoltaics (PV) capacity has shown a remarkable increase throughout the world in recent years. A PV system directly converts solar energy into DC electricity. This DC power could be directly used by DC apparatus or converted into AC power to reduce the energy purchased from the utility grid. In order to maximize the daily utilization of a PV system that incorporates energy storage with variable utility rates, it is necessary to predict a photovoltaic plant output power for different ambient conditions. The single diode model with five unknown parameters that can be derived

from manufacturers' data can be used to generate I-V characteristic curves of a single PV panel [2] [3]. With variable electric rates, a stand-alone PV setup will not fully take advantage of the usage of solar-generated electricity without the integration with energy storage. The most common ones are ice thermal storage and batteries. A natural question is which one will outperform the other in terms of economics for different situations.

Ice thermal storage has been demonstrated to perform well in terms of load shifting and peak demand shaving when TOU utility rate plans are incorporated. Many simple control strategies have been developed. Braun [4] and Drees and Braun [5] compared chiller priority, storage priority and optimal control strategies in terms of energy cost and demand charge and proposed a rule based control strategy based on heuristics . The results show that under a favorable on-peak to off-peak cost ratio a simple storage-priority strategy yields costs within 6% of optimal which significantly outperforms the chiller-priority. These simple control strategies could be easily implemented without a requirement of predictions of weather, occupancy and renewable energy information, etc.

In recent years, more sophisticated supervisory control strategies have been developed that are able to systematically curtail energy and demand expenditure when combined with predicted information for systems with thermal storage. J. Candaned et.al [6] described an approach to the formulation of a model-based predictive control (MPC) algorithm for the cooling plant of a building with ice storage under TOU utility rates. It introduces a simplified linear thermal model from a detailed building model in EnergyPlus. However, the MPC only focuses on minimizing energy cost and doesn't consider demand costs. Ma et.al [7] presented a complex MPC scheme that contains a high level MPC regulating the cooling plant with thermal storage and a low level MPC optimizing the operation of AHUs and VAV boxes. They pointed out a number of issues relating to this nonconvex MPC problem, e.g. stablity and feasibility, convergence to suboptimal solutions and computational complexity. Cox [8] proposed an approach that utilizes neural network (NN) based model predictive con-

trol strategy to be solved by the genetic algorithm (GA) optimizer. Kircher and Zhang [9] formulated a convex optimization problem including uncertainties without consideration of demand charges. Braun [10] systematically described a demand target reset algorithm that could handle a trade off between energy cost and demand charge in a suboptimal approach that could be implemented in practice.

As mentioned in [7], there are numerous issues when implementing an MPC controller in practice, including the trade off between model complexity and computational effort, and the possibility of local optimums. A model for a central cooling plant coupled with ice storage is highly nonlinear and also disjunctive due to different modes of operation for charging and discharging. A more elaborate system model can approximate real plant behaviors more precisely. However, a more complicated model is not only a computational burden, but also can deteriorate convergence to the global optimal solution. The references listed above either applied simple system models that don't consider system component capacity constraints that vary with operating conditions such that the optimal control input sequences could be solved with ease, or detailed models were utilized but solved with derivative-free optimization algorithms, e.g. particle swarm and genetic algorithm, which in general don't guarantee a global optimal solution. Lu et.al [11] developed a sophisticated plant model and compared the optimization results computed through mixed-inter nonlinear programming (MINLP) and nonlinear programming (NP). However, they didn't include demand charges and the optimization problem solver was not described explicitly. Vetterli and Benz [12] simplified the original detailed chiller model using a piece-wise linear function such that a mixed-integer linear programming could be derived for a computational simplification. However, they didn't construct a sufficiently detailed ice storage model that takes charging and discharging penalties into consideration [13].

The state of the art for battery technology enables the use of electric storage banks for both utility-scale and commercial building applications [14] [15] [16]. Rechargeable lithium-ion batteries are promising in a wide variety of fields due to their stable

charging and discharging characteristics and high round-trip efficiency behavior [17]. Integrating batteries in systems with on-site PV could provide more design and control dimensions for managing energy demand response. Nottrott et.al [18] utilized linear programming (LP) to optimize grid-connected photovoltaic-battery storage system operation. They showed that the breakeven installed cost for a lithium-ion battery is about $400-$500 per kWh. Ranaweera and Midtgard [19] investigated the economic benefits when electricity can be sold back into the grid with consideration of the impact of reverse power flow. An adjustable, time-dependent grid feed-in power limit was introduced to handle the grid voltage stability issue occurring when a large amount of power is exported to the grid. Cai et.al [20] presented a model-based predictive control approach for operation of sustainable buildings with on-site photovoltaic and battery systems that balances building utility cost and battery life. In [21], a comprehensive multi-objective optimization problem was formulated that combines cases of fast charging with excess PV power, charging for maximizing battery lifetime, charging for maximizing self-consumption, charging for maximizing self-sufficiency and charging for cost minimization. This problem was solved by using dynamic programming (DP).

Even though a large number of research publications were found that focused on optimal operation for central cooling plants coupled with ice thermal storage, and for PV systems integrated with battery storage, there appears to be very little literature on evaluating the economic performance when a central cooling plant system is integrated with on-site PV and different kinds of energy storage systems. Wang and Dennis [22] and Saffari et.al [23] explored the energy saving potential for an ice thermal storage coupled with PV. They concluded that when ice storage and solar PV are coupled together, further economic benefits could be achieved in comparison with using these two technologies independently. Savings attributed to PV only were primarily from energy cost savings, whereas the thermal storage could shift the on peak load and also improve the performance of off-grid solar PV system under variable PV generation conditions.

1.2 Motivation of combining photovoltaic with energy storage in smart grids

1.2.1 Utility rate plan structures and the net metering

Across the country, utility companies have been adopting time-of-use(TOU) energy rates and demand charges which provide incentives for consumers to manage their electric usage wisely.

Time-of-use energy rates fall into a wide range of utility rate structures which adjust the electricity cost over the course of the day. Though there are many different time-of-use rate plans, they commonly have the same intention that at times when costs of generating electricity and demand are high, the electricity rate is high. Then when costs of generating electricity and demand are low, the electricity rate is much lower. Rates may also vary from weekdays to weekends, from summer to winter.

Typical structures of time-of-use energy rates utilize different utility rates during off-peak hours and on-peak hours, and sometime partial-peak hours. Typical rate plans can include an on-peak demand charge and an any time demand charge. For the medium size commercial building considered in this study, the on-peak period is from noon to 6:00 pm, the off-peak hour is from 11:00 pm to the next day 8:00 am, and the other time is the partial-peak period. Winter typically only has off-peak and partial-peak hours with relatively lower rates than summer.

In order to maximize benefits of customers under TOU energy rates and demand charges, energy storage can be used to vary the timing of electricity usage according to utility rates.

Another innovative utility incentive policy is net energy metering (NEM) which can incentivize distributive generation technologies such as photovoltaics and wind turbines. Net energy metering provides credit to customers with solar PV systems for the full retail value of the electricity their systems generate and feed back to the grid. Electricity bills are paid annually and customers have to only pay for the net amount of electricity used from grid. Switching between a solar system's power and the utility

grid power is instantaneous such that customers never notice any interruption in the flow of power.

1.2.2 Features of energy storage devices and photovoltaics

Integrating renewable energy and energy storage systems provides a way of operating the electrical grid system more energy efficiently and stably. Thermal storage and batteries are the most common storage devices in use. One approach to integrating thermal storage on site is to use ice in combination with the cooling system. The use of ice storage can enable a change in the time variation of electrical usage for cooling in response to variations in PV availability, utility prices, and cooling requirements. Batteries can directly store electricity from excess PV generation or the grid during periods when the utility rate is low. A natural and practical question that arises is which integrated energy storage system performs better in terms of overall economics.

Ice storage has low initial and maintenance costs, but there is an efficiency penalty for charging of storage and it can only shift electrical loads associated with building cooling requirements. A battery's roundtrip efficiency, on the other hand, is quite consistent and a battery is more flexible since it can be used to shift both HVAC and non-HVAC loads. However, batteries have greater initial costs and a significantly shorter life.

1.3 Objectives and overview of methodology

This research develops a methodology and results for comparing the economic performance between central cooling systems with on-site PV coupled with different energy storage devices, i.e. ice storage and battery storage (figure 2.4, and 2.5), in terms of the life cycle cost. In order to present a fair comparison between the systems coupled with thermal storage and electric storage, an optimal system component sizing strategy and a model predictive control algorithm were developed and employed to carry out the comparisons. The present value (PV) of system costs was used as

the metric which considers cash flows over a long time line and aggregates them into the present value in order to give an investment evaluation. The life cycle economic performance for different systems depends on multiple elements such as the type of building, climate zone, utility rates, and renewable energy policies such that a simple conclusion cannot be derived. Hence a case study of a typical medium size commercial building in Riverside, California was analyzed as a guideline. Three common utility rate structures were considered: 1) time-of-use (TOU) energy with TOU demand charges; 2) TOU energy with any-time demand charges; and 3) only TOU energy charges. The situation is much more complicated when a demand charge exists since it incurs a trade off between a summation of energy costs and a single demand charge over a month. However, in practice it is not feasible to consider a monthly horizon for MPC due to prediction disturbances and heavy computational effort. Hence an innovative demand target reset algorithm was developed for MPC which converts the optimization problem into a short term horizon optimization problem. Net energy metering (NEM) is assumed that allows customers to sell back their self-generated distributive electric energy to the grid at the real-time retail price. There always exists a trade off between the model precision and computational efforts. Exceedingly elaborate system component models are not necessary for practical implementation of MPC since it would lead to a great computational effort. Therefore most of the system components were modeled based on empirical correlations or semi-empirical approaches.

The overall methodology is shown in figure 1.1. Two systems are considered: 1) the system coupled with ice storage and PV, and 2) the system coupled with batteries and PV. Firstly optimal system component sizes are determined in the optimal sizing platform. Three components were considered for each system, i.e., chiller, photovoltaic and ice storage for the first system. The second system employs batteries instead as the energy storage device. For the system coupled with ice storage, optimal component sizes are determined through a sequential optimization method, i.e., decoupling optimal control decisions and optimal sizing. For the system coupled

with batteries, a convex optimization problem was formulated that can determine optimal control decisions and component sizes in a coupled way. Then the optimal component sizes are set as inputs of model predictive controller in order to obtain an optimal control sequence. The original mixed integer nonlinear programming problem was simplified into a nonlinear programming problem that can be solved through dynamic programming. Finally the optimal life cycle costs of these two systems are computed and compared based on the optimal control sequences and simulation testbed.

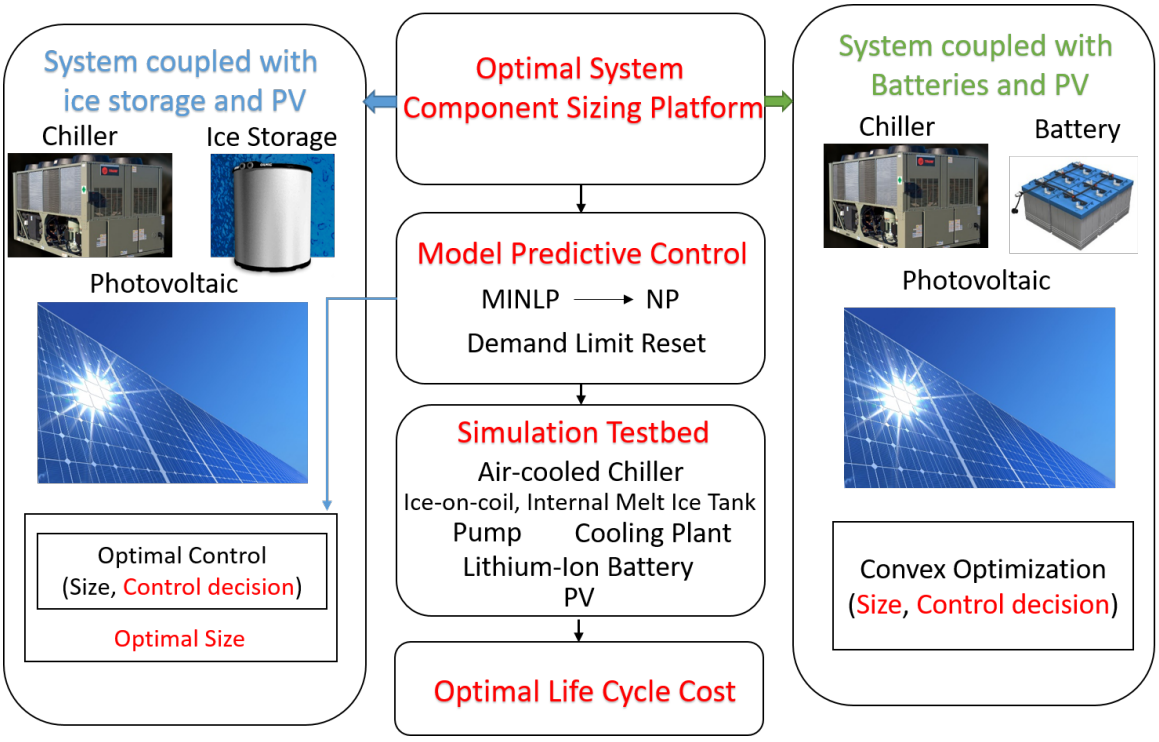

Fig. 1.1. Methodology flowchart

2. DEVELOPMENT OF SIMULATION TESTBED FOR CENTRAL COOLING SYSTEM WITH ICE STORAGE AND BATTERIES

This chapter describes details of the case study which includes site description, building model, utility rate plan and net energy metering (NEM). Then the central cooling plant models for the case study coupled with ice storage or batteries, and the photovoltaic system are presented. The case study includes a detailed cost model for determining the present value used in evaluating economic performance.

2.1 Case study description

The economic performance of the micro-grid coupled with either thermal storage or batteries depends on meteorological conditions, the building type, occupant behavior, and most importantly the utility incentives that strongly influence the model predictive control strategy that should be applied. For the purpose of presenting a methodology and guidelines for selecting the best combination of PV and energy storage, a case study in Riverside, California was analyzed. An EnergyPlus reference medium size commercial building model [24] was utilized with all parameters default to obtain an annual building load profile. Among many existing utility rate plans, three representative utility rate plans were chosen: 1) time-of-use (TOU) energy with TOU demand charges; 2) TOU energy with any time demand charges; 3) only TOU energy charges. These utility rate structures were implemented under a net energy metering (NEM) policy adopted in California that allows customers to sell back their self-generated renewable energy into the conventional grid at retail prices.

2.1.1 Site description

The case study used Riverside, California as the location with meteorological data extracted from the Typical Meteorological Year (TMY3) data set. Its latitude is 33.95 N and longitude is 117.38 W. This is a hot semi-arid climate with hot summers and warm to cool winters, and with minimal precipitation. The location was chosen to minimize the influence of heating on the overall economic performance evaluation. In order to have a fair comparison between thermal storage and electric storage, it was assumed that both systems use natural gas for heating. If a heat pump for heating were utilized, batteries could play a load shifting role whereas the ice storage could not.

2.1.2 Building model

A medium size commercial building model (figure 2.1) was extracted from the EnergyPlus prototypical building library [25] and all the parameters were set as default. The building has three floors with 53,600 sq feet of floor area. Windows are evenly distributed along four facades with a 33% window fraction. The detailed setup for the architecture, interior loads and schedules were unchanged. An annual building cooling load profile (HVAC load) and electric loads associated with other devices (non-HVAC loads) were computed and used as inputs to an optimal component sizing platform, and simulation testbed that incorporated an MPC algorithm. For this reference model, the design day building load profile is shown in figure 2.2. The maximum cooling load occurs on September 11th which is 226kW and the design day total cooling load is 2836.75 kWh. The dash line represents the scaled utility rates for off-peak, partial-peak and on-peak periods.

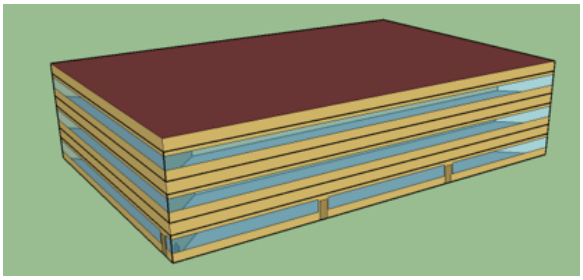

Fig. 2.1. Building model

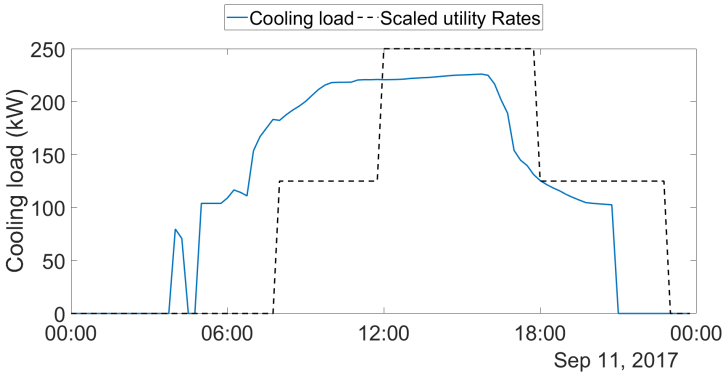

Fig. 2.2. Design day cooling load profile

2.1.3 Utility rate plan

The utility rate plays the most decisive role in affecting the economic benefit of integrating energy storage into the system in this case study. When investors adopt energy storage, the utility rate should have a high enough on-peak to off-peak rate ratio and/or demand charge to overcome additional upfront costs. A TOU rate is a plan whose rates vary according to the time of day, season, and day type (weekday or weekend/holiday). Higher rates are charged during the peak demand hours and lower rates occur during low demand hours. Rates are typically higher in summer than winter. The case study used 2017 calendar information to set the weekdays and weekends schedule.

The overall cost savings potential of load shifting with the help of energy storage is naturally determined by the kinds of TOU rate being used. In this study, three representative California TOU rates were chosen that are summarized in table 2.1. Demand costs were determined based on 1 hour average power and TOU energy costs were charged based on 15-minute energy flows. The monthly utility bill can be computed based on equation 2.1.

$$\sum_{i=0}^{N_e-1} E(i)P_{tb}^{15}(i)\Delta T + max(D(k)P_{tb}^{60}(k)|k \in \{0,\ldots,N_d-1\}) \tag{2.1}$$

where N_e is the number of 15-minute time intervals, E is the time of use energy rate, P_{tb}^{15} is the 15-minute average total building electrical load, ΔT is the time step, D is the demand charge rate, P_{tb}^{60} is the 60-minute average total building electrical load and N_d is the number of hourly time intervals.

The utility rate PG&E A10 has an any-time demand charge which might cause the cost saving coming from demand charges by load shifting to be small. However the on-peak to off-peak energy rate ratio in summer is about 1.6 which is the primary cost saving potential driver. The utility rate SCE GS-2B also has a significant on-peak to off-peak energy cost ratio in summer of 2.1, and also has a TOU demand cost rate. SCE GS-R is quite different in that it doesn't have a demand charge. However its on-peak to off-peak energy cost ratio is about 5.5 providing a significant incentive for use of storage.

2.1.4 Net energy metering

The Net Energy Metering 2.0 (NEM) is an established policy in California that is continually adapted. Customers with eligible renewable generation facilities installed behind the customers' meters that meet technical requirements are able to participate in the NEM tariff.

Under NEM, customer-generators offset their charges for any consumption of electricity provided directly by their renewable energy facilities and receive a cumulative financial credit monthly for the power generated by their on-site renewable energy

systems that is fed back into the power grid for use by other utility customers over the course of a billing cycle. The unique speciality of NEM is that the credits are valued at the same price that customers would otherwise be charged for electricity consumed. At the end of every year that a customer-generator has been on the NEM tariff, the credits and charges accrued over the previous 12-month billing period are "trued-up".

The features of NEM are pivotal in the optimization problem considered in this study since the sell-back and purchasing price of electricity are the same, only the net power purchased from the grid needs to be computed for the optimization. Also, there is an annual "true up" at the end of the billing year which means any excess self energy generation is not beneficial, even though some net metering programs might have "net surplus compensation " under certain conditions but with a negligible rate. This fact certainly guides the optimal sizing problem, i.e., setting an upper bound for PV size.

In this study, we assumed that any excess generated energy at the end of the billing year was wasted. Other fees associated with the NEM program enrollment, such as interconnection fee and non-bypassable charges were assumed to be small and the same for all cases, thus were not considered in the formulation of the optimization problem.

2.1.5 Life cycle financial performance metric

In this study, we selected the Present Value (PV) as the metric to evaluate the life cycle cost performance of different systems coupled with ice storage or batteries. The Present Value is a straightforward variable that aggregates cash flows happening during the course of a time-line in the future that investors are interested in. The Present Value of system costs is calculated based on equation 2.2.

$$SC_{PV} = \sum_{t=1}^{n} R_t (\frac{1+i}{1+d})^t + C_{ii} \tag{2.2}$$

Table 2.1.
TOU utility rate plans

TOU Energy Rate ($/kWh)						
	PG&E A10		SCE GS-2B		SCE GS-R	
Summer	On-Peak	0.22455	On-Peak	0.12280	On-Peak	0.39056
	Partial-Peak	0.16942	Partial-Peak	0.08040	Partial-Peak	0.13509
	Off-Peak	0.14135	Off-Peak	0.05772	Off-Peak	0.0707
Winter	Partial-Peak	0.14107	Partial-Peak	0.07664	Partial-Peak	0.08962
	Off-Peak	0.12400	Off-Peak	0.06514	Off-Peak	0.07812
Demand Charge Rate ($/kW)						
	PG&E A10		SCE GS-2B		SCE GS-R	
Summer	Any-time	19.13	On-Peak	19.61	Any-time	0
			Partial-Peak	3.83		
			Off-Peak	0		
Winter	Any-time	11.24	Any-time	0	Any-time	0

where R_t is the system operation and maintenance costs during a single period t, i is the inflation rate, d is the discount rate, n is the number of time periods and C_{ii} is the initial investment. The parameter values to be considered in this study are listed in table 2.2.

Table 2.2.
Present value parameter assumption

Parameter	Value
i	2%
d	7%
n	10

2.1.6 Installed costs of system components

The installed cost of the system either coupled with ice storage or batteries is a pivotal factor that determines not only the sizing but also the overall life cycle cost. Therefore it is an essential and fundamental parameter in the study.

For the chiller and ice storage, since these two components are already well developed, the installed prices are quite stable and low compared with batteries. In contrast, the costs of renewable energy such as photovolotaics and the associated battery storage are changing because they are less mature and still under development. Hence an analysis based on the current installed costs might be not comprehensive and persuasive. Consequently, the current installed costs are used as a benchmark followed by a parametric study of installed cost values in the study.

Chiller and ice storage installed costs

The installed cost of cool thermal energy storage used in this study is based on a report from DOE [26]. Considering the influence of inflation and assuming an inflation

rate of 7%, table 2.3 shows the adjusted installed cost estimates for different storage media.

Table 2.3.
Thermal energy storage cost estimates

Storage Medium	Chiller $/ton	Installed Tank Cost $/ton-hour
Chilled Water	421∼631	63∼210
Ice on coil, internal melt	421∼1052	105∼147
Ice Harvester	2,315∼3,157	42∼63
Encapsulated Ice	421∼1052	105∼147
PCM	421∼631	210∼315

The storage medium of this study is ice on coil, internal melt. Thus the installed cost of a chiller and ice storage were chosen as the mean value of each cost range, i.e. 735 $/ton for a chiller and 126 $/ton-hour for an ice tank.

Battery storage installed costs

The installed costs for batteries depend on the battery material, battery power capacity and battery energy storage capacity. Battery power capacity and battery energy storage capacity can be represented by a single parameter called duration, which is the ratio of energy storage capacity to power capacity. The classification of battery storage duration is short duration (<0.5 hours), medium-duration (0.5∼2 hours) and long-duration (>2 hours).

For cost information we referred to a report from the National Renewable Energy Laboratory [14]. As discussed in chapter 2, this study assumes lithium-ion batteries because of their stable and reliable operation characteristics. For a commercial building scale Li-ion storage system (10∼1000kW), batteries should be classified as long-duration storage.

Batteries installed cost consists of two parts which are energy capacity cost ($/kWh) and power capacity cost ($/kW). For a 2-hour duration battery, the energy capacity cost is 454 $/kWh and the power capacity cost is 910 $/kW [15]. If the battery C-rate is 0.5, i.e., the ratio of battery discharging rate to its maximum capacity, the installed cost for a lithium-ion battery, in terms of $/kWh, is 909 $/kWh.

Photovoltaics installed cost

Solar photovoltaic (PV) deployment has grown rapidly in the United States over the past several years due to the rapid decreasing initial cost. Figure 2.3 shows that current commercial building PV system installed costs are about one third of the cost ten years ago. This dramatic cost drop makes the application of PV for distributed generation more intriguing and promising at present and in the future. Since the simulation case study assumes the year 2017, the installed cost was taken to be 1.88 $ per peak watt.

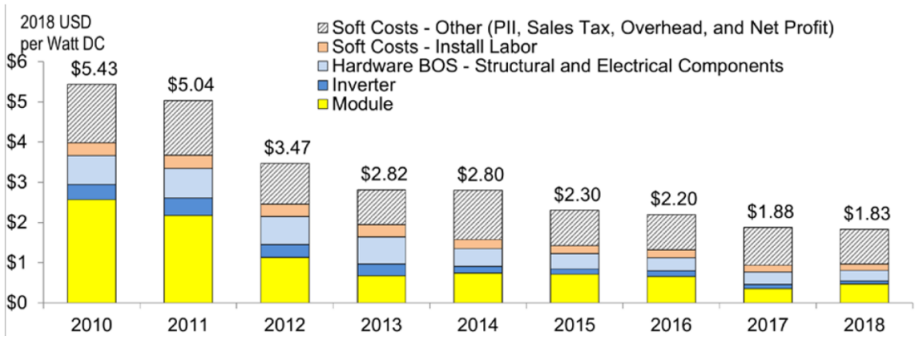

Fig. 2.3. Commercial PV system cost benchmark summary [15]

2.1.7 Maintenance costs

Since the economic performance only considers a ten-year time horizon, this study only includes maintenance costs without replacement. The maintenance costs for the PV system is taken to be 18 $/kW per year, which means the overall maintenance

costs for ten years are about 10 % of the PV installed cost [15]. For lithium-ion batteries, the maintenance costs are taken to be 7.8 $/kW per year [14], which could be converted to 3.9 $/kWh per year with a 0.5 C-rate. This corresponds to maintenance costs for lithium-ion batteries of about 4.3 % of their installed cost in terms of a ten-year operating duration. The maintenance cost of a cooling plant is considered as 2% of the installed cost.

2.2 Micro-grid system layout

Figure 2.4 gives a micro-grid component layout of the building, central cooling plant coupled with ice storage and PV system to be considered in this study. Under the California net energy metering 2.0 policy, customers can export their self-generated energy back to the grid at retail prices. It allows power bi-directional flows between the traditional power grid and micro-grid which effectively integrates distributed generation, especially renewable energy sources, into the conventional electric grid. In this system, electricity used to charge ice storage can be from the power grid or on-site PV depending on the economic benefits from utility rates, cooling plant performance and cooling loads. Electricity generated by PV panels can be directly consumed or exported to the power grid. Figure 2.5 shows a different smart grid component layout comprising the building, conventional central cooling plant, battery bank, power grid, and PV array, which will be compared with the system of figure 2.4. This system contains a battery bank as energy storage instead of ice storage tanks. Batteries can be charged from the power grid or customer owned on-site PV. They can also discharge electric power to support on-site consumption or sales back to the power grid to take advantage of favorable utility rates.

2.3 Central cooling system modeling

This section describes the central cooling plant system configuration and component models used in this work. We refer to a project report [27]. For the case in figure

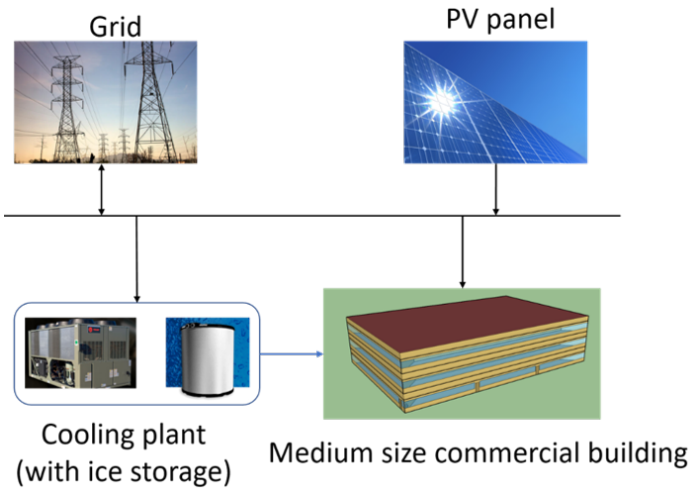

Fig. 2.4. On-Site PV coupled with Ice Storage and Cooling System

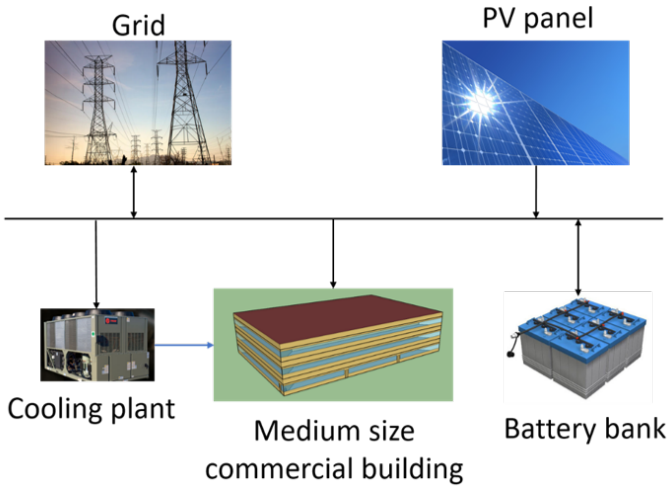

Fig. 2.5. On-Site PV coupled with Battery Storage

2.4, there are several well-developed ice storage system configurations, including the ice tanks and chillers in a parallel configuration, ice tanks and chillers in series with chillers downstream, and a series configuration but with chillers being upstream of storage. The last one is considered throughout this research since it allows the chiller to operate at a relatively higher evaporating temperature for a higher COP. Hence this popular system configuration shown in figure 2.6 was chosen for the simulation case studies. The baseline system for the case study has a 52-ton air-cooled chiller

with 30% propylene glycol and 70% water in the circulating loop, 4 single-stage scroll compressors, two refrigeration circuits and two 250 ton-hour identical ice tanks. The baseline component capacities are scaled when addressing optimal sizing in this study.

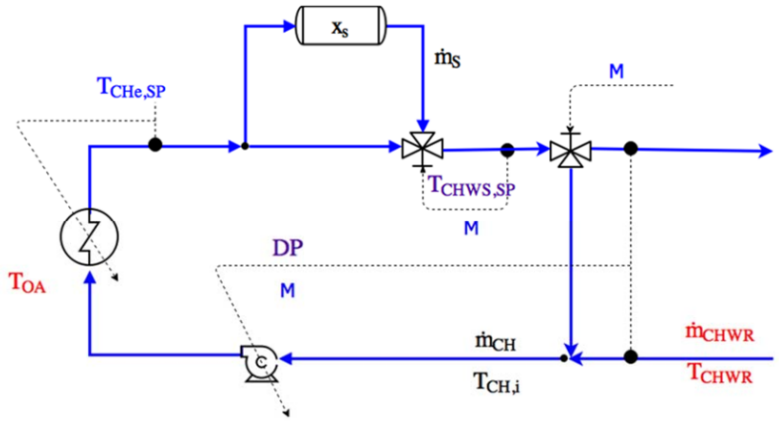

Fig. 2.6. Schematic of ice storage chiller plant and nomenclature

Table 2.4.
Nomenclature

M:	plant modes (off,chiller only, ice only, chiller and ice, freezing)
DP:	pressure differentials
T_{OA}:	outdoor dry bulb temperature $[°C]$
$T_{CHe,SP}$:	chiller exit temperature setpoint $[°C]$
$T_{CHWS,SP}$:	primary chilled water supply temperature setpoint $[°C]$
$T_{CH,i}$:	chiller inlet temperature $[°C]$
T_{CHWR}:	return water temperature from building $[°C]$
$\dot{m}_s$:	mass flow rate passing two ice storage tanks $[kg/s]$
$\dot{m}_{CH}$:	mass flow rate passing chiller $[kg/s]$
$\dot{m}_{CHWR}$:	mass flow rate from buildings $[kg/s]$
x_s:	ice storage state of charge

2.3.1 Ice storage model

In this study, ice tanks utilized an internal-melt, ice-on-coil configuration. For this type of ice storage device, we refer to the semi-empirical model developed by West and Braun (1998). With the help of heat exchanger effectiveness, at any stage, the maximum charging and discharging rates can be expressed as:

$$Q_{IS} = \epsilon_D(x_s)\dot{m}_s C_{p,w}(T_{s,i} - T_{fr}) \quad (T_{s,i} > T_{fr}) \tag{2.3}$$

$$Q_{IS} = \epsilon_C(x_s)\dot{m}_s C_{p,w}(T_{fr} - T_{s,i}) \quad (T_{s,i} \leq T_{fr}) \tag{2.4}$$

where $T_{s,i}$ is the water/glycol mixture fluid ice storage inlet temperature, ϵ_D and ϵ_C are the heat transfer effectiveness for discharging and charging which are a function of the state of charge (x_s) for a given mass flow rate. T_{fr} is the freezing point temperature (0°C for water). The storage model neglects any heat gains through the storage shell and treats the storage as a lumped system whose state can be denoted by a single variable, i.e., state of charge (SOC), which is defined as:

$$x_s = \frac{u_f - u}{u_{sf}} \tag{2.5}$$

where u is the specific internal energy of the water and ice mixture in the tank, u_f is internal energy of saturated liquid water, and u_{sf} is the latent heat of fusion for ice. Hence the energy balance of ice storage is as follows:

$$\dot{x}_s = \frac{Q_{IS}}{C_s} \tag{2.6}$$

Combining equation 2.3, 2.4 and 2.6 leads to a lumped dynamic model of ice storage in equation 2.7 and equation 2.8.

$$\dot{x}_s = \frac{\epsilon_D(x)\dot{m}_s C_{p,w}(T_{s,i} - T_{fr})}{C_s} \quad (T_{s,i} > T_{fr}) \tag{2.7}$$

$$\dot{x}_s = \frac{\epsilon_C(x)\dot{m}_s C_{p,w}(T_{fr} - T_{s,i})}{C_s} \quad (T_{s,i} \leq T_{fr}) \tag{2.8}$$

The two dynamic equations require a model for heat transfer effectiveness during charging and discharging. West and Braun (1999) used a polynomial to correlate

charging and discharging effectiveness in terms of state of charge or discharge of the form in equation 2.9

$$\epsilon(x_s) = a_0 + a_1 x_s + a_2 x_s^2 + \dots \tag{2.9}$$

The heat transfer effectiveness behavior as a function of state of charge during charging and discharging is depicted in figure 2.7. For the charging process, at the beginning, heat transfer effectiveness is relatively constant over a large range. This is because the ice thickness on the tubes is relatively small and ice formations on adjacent tubes do not intersect. However, during the last stage of charging, ice formations begin overlapping with others, which causes a significant loss of heat transfer area. This phenomenon causes a rapid decrease of heat transfer effectiveness. The behavior also happens for the discharging process. The heat transfer effectiveness is relatively constant with decreasing at the beginning which is followed by a rapid drop at the last stage. The overlapping water layers cause the later dramatic decreasing in the heat transfer effectiveness with decreasing state of charge.

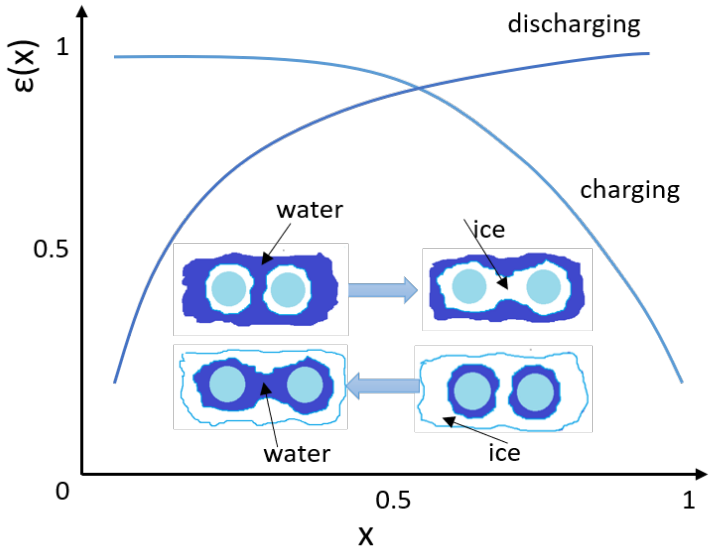

Fig. 2.7. Schematic of ice storage heat transfer effectiveness behavior

However, the heat transfer effectiveness of equation 2.9 is a function of state of charge assuming a fixed flow rate. When flow rate varies, the heat transfer effectiveness varies with not only state of charge but also mass flow rate. The temperature profile through ice tanks' pipes has the shape in figure 2.8. For this kind of heat transfer problem, the lumped ϵ-NTU model structure in equation 2.10 can capture the overall behavior for a single ice tank.

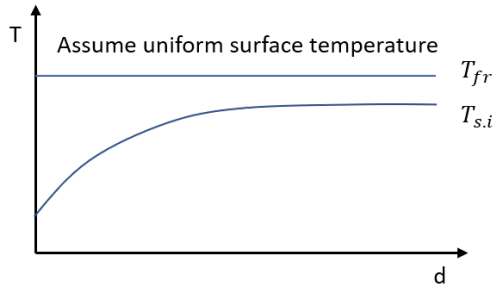

Fig. 2.8. Schematic of ice storage heat transfer temperature profile

$$\epsilon(\frac{\dot{m}_s}{N_s}, x_s) = 1 - e^{-NTU(\frac{\dot{m}_s}{N_s}, x_s)} \tag{2.10}$$

The NTU is the ratio of the overall thermal resistance between the chilled water and ice storage (UA) to the heat capacity rate ($\frac{\dot{m}_s}{N_s}C_{p,w}$). The thermal resistance UA is a function of state of charge describing how the overall thermal resistance between the chilled water and ice storage varies depending on the formation or melting of ice. Then the heat transfer effectiveness can be expressed as in equation 2.11. Based on this representation, we can retrieve functional forms for UA and $\epsilon(\frac{\dot{m}_s}{N_s}, x_s)$ from a dataset measured at a fixed flow rate [27].

$$\epsilon(\frac{\dot{m}_s}{N_s}, x_s) = 1 - e^{-\frac{UA(x_s)}{\frac{\dot{m}_s}{N_s}C_{p,w}}} \tag{2.11}$$

The empirical polynomial representation of heat transfer effectiveness for a fixed flow rate is expressed in equation 2.12 where the subscript 0 denotes a fixed flow rate for the experiments.

$$\epsilon_0(x_s) = a_0 + a_1 x_s + a_2 x_s^2 + \dots \tag{2.12}$$

From equation 2.11, the function $UA(x)$ has the following form obtained for the test flow rate

$$UA(x_s) = -\frac{\dot{m}_{s,0}}{N_s} C_{p,w} ln(1 - \epsilon_0(x_s)) \tag{2.13}$$

Finally, by combining equations 2.11 and 2.13, a heat transfer effectiveness model as a function of mass flow rate and state of charge was obtained as:

$$\epsilon(\frac{\dot{m}_s}{N_s}, x_s) = 1 - (1 - \epsilon_0(x_s))^{\frac{\dot{m}_{s,0}}{\dot{m}_s}} \tag{2.14}$$

The charging and discharging heat transfer effectiveness regression representations for a fixed flow rate with the 250 ton-hour ice storage tank at 4.4877 kg/s (57.4 gpm) are given in equations 2.15. With these two polynomial regression models tuned for a fixed experimental mass flow rate data set, heat transfer effectivenesses for charging and discharging at different mass flow rates could be extracted.

$$\begin{aligned}
\epsilon_{C,0}(x_s) &= -8.5333x_s^5 + 14.8774x_s^4 - 8.4289x_s^3 + 1.3921x_s^2 - 0.2911x_s + 0.9839 \\
\epsilon_{D,0}(x_s) &= 19.9760x_s^5 - 56.1250x_s^4 + 58.9749x_s^3 - 28.2980x_s^2 + 6.3670x_s + 0.1217
\end{aligned} \tag{2.15}$$

2.3.2 Air-cooled chiller model

A chiller model was obtained by regression using experimental data. Open-loop model and closed-loop models were developed [27]. The open-loop model means there is no control of the chiller outlet temperature setpoint and compressor stage is an input. For this model, the maximum chiller capacity and corresponding power are a function of chiller inlet temperature ($T_{CH,i}$), brine mass flow rate ($\dot{m}_{CH}$), ambient dry bulb temperature (T_{OA}) and compressor stage.

$$\begin{bmatrix} P_{CH,OL} \\ Q_{CH,OL} \end{bmatrix} = f_{OL}(T_{CH,i}, \dot{m}_{CH}, T_{OA}, Stage) \tag{2.16}$$

The closed-loop model is applied to the case where the chiller outlet temperature is controlled to its setpoint ($T_{CHe,SP}$) through control of the compressor stage.

$$P_{CH,CL} = f_{CL}(Q_{CHL}, T_{CHe,SP}, T_{OA}) \tag{2.17}$$

The open loop chiller model gives maximum chiller cooling capacity which is used as a constraint in the optimization problem formulation, whereas the closed loop chiller model describes the required power to meet a chiller outlet temperature setpoint. Equations 2.18-2.20 are second order polynomials that were determined through least-squares.

$$Q_{CH,OL} = 87.4537 + 4.1228T_{CH,i} + 11.1804\dot{m}_{CH} + 0.2256T_{OA} + 0.0194T_{CH,i}^2 - 0.4630\dot{m}_{CH}^2 - 0.0153T_{OA}^2 + 0.1293T_{CH,i}\dot{m}_{CH} - 0.0390T_{CH,i}T_{OA} - 0.0663T_{OA}\dot{m}_{CH} \tag{2.18}$$

$$P_{CH,OL} = 30.6853 + 0.1525T_{CH,i} + 0.7983\dot{m}_{CH} + 0.2208T_{OA} + 0.0024T_{CH,i}^2 - 0.0396\dot{m}_{CH}^2 + 0.0108T_{OA}^2 + 0.0105T_{CH,i}\dot{m}_{CH} + 0.0049T_{CH,i}T_{OA} + 0.0009T_{OA}\dot{m}_{CH} \tag{2.19}$$

$$P_{CH,CL} = 2.2586 + 0.1737Q_{CHL} + 0.0138T_{CHe,SP} - 0.3455T_{OA} + 0.0001Q_{CHL}^2 + 0.0123T_{CHe,SP}^2 + 0.0096T_{OA}^2 - 0.0063Q_{CHL}T_{CHeS,P} + 0.0056Q_{CHL}T_{OA} - 0.0103T_{CHe,SP}T_{OA} \tag{2.20}$$

2.3.3 Pump model

A detailed model of the distribution system is not necessary and will not be employed for the purpose of this work because it would require detailed knowledge of valve and pump characteristics and pipe geometries, and pump power is relatively small compared to other power consumption in the system. Instead, a simple empirical model is employed that relates pump power consumption to flow rate:

$$P_{pump} = \frac{V_f(DP)}{\eta_{pump}\eta_{motor}\eta_{inverter}} \tag{2.21}$$

where V_f is volume flow rate (m^3/s) and DP is the pressure difference between supply and return pipes. Pressure differences primarily depend on the chiller mode and were obtained from manufacturers' data. The DP of "Off", "Chiller only", "Ice storage only", "Chiller and ice storage", "Freezing" are 0, 6.4830, 12.3913, 6.3493. 4.9482 psi

respectively. η_{pump}, η_{motor} and $\eta_{inverter}$ are 0.4, 0.9 and 0.95 respectively, which also were obtained from manufacturers' data [27].

2.3.4 Central cooling plant modeling

The central cooling plant model for the system coupled with ice storage is more complicated than the system coupled with batteries since there are five plant modes in total: "Chiller plant off (OFF)", "Chiller only (CH)", "Ice cooling (discharging) only (I)", "Chiller and Ice cooling (CHI)" and "Freezing (charging) ice (F)". A mode where the chiller meets the cooling load and charging storage at the same time ("Chiller and Freezing") is not considered due to low COP and high operating cost. For the system coupled with battery storage, only modes "Chiller plant off (OFF)" and "Chiller only (CH)" are considered.

The plant model predicts outputs and states according to cooling load (CWL), outdoor dry bulb temperature (T_{OA}) and other parameters and conditions with control decisions of chiller outlet temperature setpoint ($T_{CHe,SP}$) and plant modes (M). The overall plant model has the following discrete time form [27]:

$$[x_s(k+1), y(k)] = plantmodel(x_s, T_{CHe,SP}, M, \dot{m}_{CHWR}, CWL, T_{OA}, T_{CHWS,SP}, DP, Maxstage, \Delta t)_k$$
$$y(k) = [T_{CH,i}, T_{CH,e}, T_{s,e}, \dot{m}_s, Q_{CH}, Q_{CHL}, Q_{CH,max}, P_{CH}, Q_{IS}, Q_{ISL}, Q_{IS,max}, P_{pump}]_k \tag{2.22}$$

where maximum chiller capacity ($Q_{CH,max}$) is defined as the heat transfer rate from water/glycol to the chiller with full stage compressors and ice storage cooling load (Q_{ISL}) is defined by the required heat transfer rate to meet a given setpoint for the primary supply water temperature. The ice storage cooling capacity (Q_{IS}) is the heat transfer rate from water/glycol to the tank. Maximum ice storage capacity ($Q_{IS,max}$) occurs when the mixing valve of the tank is fully open to the tank when all of mass flow goes through ice storage. Cooling loads, capacities and maximum capacities are distinguished in the model for cases where the chiller and ice storage do not have

enough capacities to meet their loads. When they are able to meet their loads, cooling capacities are equal to cooling loads.

OFF mode

When the mode is OFF, temperatures are not available since pumps are off. The governing equations for this mode are as follows:

$$\begin{aligned} &\dot{m}_{CH,i} = 0 \quad \dot{m}_s = 0 \quad P_{CH} = 0 \quad Q_{CH} = 0 \\ &Q_{CHL} = 0 \quad Q_{IS} = 0 \quad Q_{ISL} = 0 \end{aligned} \tag{2.23}$$

Chiller only mode

Firstly, the open-loop model is applied to calculate maximum chiller cooling capacity. Next the chiller load defined by the chiller outlet temperature setpoint $T_{CHe,SP}$ is calculated compared with the maximum chiller cooling capacity. If the maximum chiller cooling capacity is larger than the chiller cooling load, then chiller cooling capacity equals chiller cooling load and the setpoint $T_{CHe,SP}$ can be achieved. If the chiller lacks enough cooling capacity, then chiller cooling load is its maximum cooling capacity and the setpoint $T_{CHe,SP}$ can not be met. This time the chiller outlet

temperature T_{CHe} is calculated based on chiller capacity, inlet temperature and mass flow rate.

$$
\begin{aligned}
T_{CHWR} &= T_{CHWS,SP} + \frac{CWL}{\dot{m}_{CHWR} C_{p,w}} \\
T_{CH,i} &= T_{CHWR} \\
T_{CHe,SP} &= T_{CHWS,SP} \\
T_{CH,e} &= T_{CHe,SP} \quad (if \quad Q_{CHL} \leq Q_{CH,max}) \\
&= T_{CH,i} - \frac{Q_{CH,max}}{\dot{m}_{CH,i} C_{p,w}} \quad (if \quad Q_{CHL} > Q_{CH,max}) \\
T_{CHWS} &= T_{CH,e} \\
\dot{m}_{CH,i} &= \dot{m}_{CHWR} \\
\dot{m}_s &= 0 \\
P_{CH} &= f_{CH,CL}(Q_{CHL}, T_{CHe,SP}, T_{OA}) \quad (if \quad Q_{CHL} \leq Q_{CH,max}) \\
&= f_{CH,OL}(T_{CH,i}, \dot{m}_{CH,i}, T_{OA}, maxstage) \quad (if \quad Q_{CHL} > Q_{CH,max}) \\
Q_{CH} &= Q_{CHL} \quad (if \quad Q_{CHL} \leq Q_{CH,max}) \\
&= Q_{CH,max} \quad (if \quad Q_{CHL} > Q_{CH,max}) \\
Q_{CHL} &= \dot{m}_{CH,i} C_{p,w} (T_{CH,i} - T_{CHe,SP}) \\
Q_{CH,max} &= g_{CH,OL}(T_{CH,i} \dot{m}_{CH,i}, T_{OA}, maxstage) \\
Q_{IS} &= 0 \\
Q_{ISL} &= 0
\end{aligned}
\tag{2.24}
$$

Ice cooling (discharging) only mode

Firstly, maximum ice storage cooling capacity ($Q_{IS,max}$), i.e. all of the brine flow passing through the tank, is calculated. Then this value is compared with the ice storage load (Q_{ISL}). If the load is greater than the capacity, the mass flow rate that goes through the ice tanks ($\dot{m}_s$) is set to the maximum flow rate ($\dot{m}_{CH,i}$). Otherwise,

when the load is smaller than the capacity, $\dot{m}_s$ is adjusted until the ice storage cooling capacity matches the load. The governing equations for the ice mode are shown below:

$$
\begin{aligned}
T_{CHWR} &= T_{CHWS,SP} + \frac{CWL}{\dot{m}_{CHWR} C_{p,w}} \\
T_{CHe,SP} &= T_{CHWR} \\
T_{CH,i} &= T_{CHWR} \\
T_{CH,e} &= T_{CH,i} \\
T_{CHWS} &= (1 - \frac{\dot{m}_s}{\dot{m}_{CH,i}}) T_{CH,e} + \frac{\dot{m}_s}{\dot{m}_{CH,i}} T_{s,e} \\
T_{s,e} &= T_{CH,e} - \frac{Q_{IS}}{\dot{m}_s C_{p,w}} \\
\dot{m}_{CH,i} &= \dot{m}_{CHWR} \\
\dot{m}_s &= \dot{m}_{CH,i} \quad (if \quad Q_{IS,max} \leq Q_{ISL}) \\
&= iteration \quad until \quad Q_{IS} = Q_{ISL} \quad (if \quad Q_{IS,max} > Q_{ISL}) \\
P_{CH} &= 0 \\
Q_{CH} &= 0 \\
Q_{CHL} &= 0 \\
Q_{IS} &= N_s(\epsilon_D(\frac{\dot{m}_s}{N_s}, x_s) \frac{\dot{m}_s}{N_s} C_P (T_{CH,e} - 0)) \quad (if \quad Q_{ISL} \leq Q_{IS,max}) \\
&= Q_{IS,max} \quad (if \quad Q_{ISL} > Q_{IS,max}) \\
Q_{ISL} &= \dot{m}_{CH,i} C_{p,w} (T_{CH,e} - T_{CHWS,SP}) \\
Q_{IS,max} &= N_s(\epsilon_D(\frac{\dot{m}_{CH,i}}{N_s}, x_s) \frac{\dot{m}_{CH,i}}{N_s} C_{p,w} (T_{CH,e} - 0))
\end{aligned}
\tag{2.25}
$$

Chiller and ice cooling mode

For chiller and ice mode, the plant governing equations are the combination of equations 2.24 and 2.25. The difference here compared with chiller only and ice only modes is that the chiller outlet setpoint ($T_{CHe,SP}$) in this case is determined by a controller. In chiller only mode $T_{CHe,SP}$ is set at 44 °F and in ice only mode it is

same as chilled water return temperature (T_{CHWR}). The chiller load and ice storage load are calculated based on $T_{CHe,SP}$.

Freeze mode (charging)

For the freeze mode, the chiller operates at maximum capacity with all stages. In this case, both $T_{CH,i}$ and $T_{CH,e}$ are unknown. Hence, $T_{CH,e}$ is adjusted until $Q_{CH,max}$ and $Q_{IS,CR}$ match each other, where $Q_{IS,CR}$ is the charging rate, i.e. $Q_{IS,CR} = -Q_{IS}$.

$$\begin{aligned}
T_{CH,i} &= T_{s,e} \\
T_{CH,e} &= \quad iteration \quad until \quad Q_{CH,max} = Q_{IS,CR} \\
T_{s,e} &= T_{CH,e} + \frac{Q_{IS,CR}}{\dot{m}_s C_{p,w}} \\
\dot{m}_s &= \dot{m}_{CH,i} \\
P_{CH} &= f_{CH,OL}(T_{CH,i}, \dot{m}_{CH,i}, T_{OA}, maxstage) \\
Q_{CH} &= Q_{CH,max} \\
Q_{CHL} &= Q_{CH,max} \\
Q_{CH,max} &= g_{CH,OL}(T_{CH}, \dot{m}_{CH,i}, T_{OA}, maxstage) \\
Q_{IS,CR} &= N_s(\epsilon_c(\frac{\dot{m}_s}{N_s}, x_s)\frac{\dot{m}_s}{N_s} C_{p,w}(0 - T_{CH,e}) \\
fsQ_{IS} &= -Q_{IS,CR} \\
Q_{ISL} &= 0
\end{aligned} \tag{2.26}$$

2.4 Battery storage and photovoltaics modeling

2.4.1 Battery model

The battery dynamics can also be approximated by the concept of state of charge:

$$\dot{x}_b = \frac{I}{Q_{bat,I}} \tag{2.27}$$

The discrete time model is shown below:

$$x_b(k+1) = x_b(k) + \frac{I(k)\Delta t}{Q_{bat,I}} \tag{2.28}$$

where I (Amp) is the current and positive for charging and negative for discharging, $Q_{bat,I}$ (Amp-hr) is the battery current capacity and Δt is the time step. It is important to note for a battery that state of charge is defined by the ratio of how many electrons are stored in the battery to the total storage capacity. Hence in order to obtain an electric power relation, it is necessary to multiply both the numerator and denominator of $\frac{I(k)\Delta t}{Q_{bat,I}}$ by voltage with the result shown in equation 2.29,

$$x_b(k+1) = x_b(k) + \frac{P_b(k)\Delta t}{Q_{bat}} \tag{2.29}$$

This simple state of charge model assumes constant voltage during charging and discharging. For a lead-acid battery, voltage varies significantly during these two processes. For a lithium-ion battery, even though battery performance is much better than for a lead-acid, which means voltage variation in a certain state of charge range is small (3.2%) (see figure 2.9(a)), a constant voltage assumption causes difficulties when applied in a model predictive control platform. This is because a constant voltage assumption leads to no penalty for battery charging and discharging performance at different states of charge and current magnitudes, which leads to a lack of unique solutions for MPC.

To overcome this issue, a detailed lithium-ion battery model from MATLAB Simulink Electric Drives/Extra Sources library was used to obtain a linearly interpolated battery model based on a typical battery's charging and discharging characteristics (figure 2.9). Figure 2.9(a) shows the charging behavior of a lithium-ion battery with 130 amp-hour capacity and 0.5 C-rate.(C-rate is a measure of the rate at which a battery is discharged relative to its maximum capacity. A 1C rate means that the discharge current will discharge the entire battery in 1 hour).

The inputs of the MATLAB Simulink lithium-ion battery model are charging (discharging) current ($I(k)$), initial state of charge ($x_b(k)$) and simulation time duration

(Δt). The outputs are voltage (V) and state of charge (x_b) variations from time $k\Delta t$ to $(k+1)\Delta t$. By integration of voltage and current, battery averaged charging and discharging power over time duration (Δt) can be computed. The overall linearly interpolated battery model has the form in equation 2.30.

$$\begin{bmatrix} x_b(k+1) \\ P_b(k) \end{bmatrix} = F(I(k), x_b(k), \Delta t) \tag{2.30}$$

where $P_b(k)$ represents the averaged battery power over time Δt. For the model predictive control algorithm Δt is one hour and for the system simulation testbed Δt is 15 minutes. To prevent low and high states of charge, the state of charge is subjected to the constraint in equation 2.31.

$$25\% \leq x_b(k) \leq 95\% \tag{2.31}$$

For a given time step with a constant current, i.e. 1 hour for MPC and 15 minutes for the simulation testbed, there is a region of current and initial state of charge that allows the final state of charge to be within the 25% to 95% constraint, and other combinations are not feasible. Figure 2.10 shows the two feasible input regions used in this study for 1 hour and 15-minute time steps. Positive current means charging and negative means discharging. With a low initial state of charge, the battery can be charged with a high current, and with a high initial state of charge, it can be discharged with high current. Notice that the feasible region is much larger for the 15-minute than the 1-hour time step since a shorter time duration allows higher charging and discharging rates.

2.4.2 Photovoltaics model

A photovoltaic system converts sunlight into DC electricity that can be used on site or support other grid users when extra generated electricity is available. The fundamental element is a PV cell which can be grouped into PV arrays and panels. A PV cell is a semiconductor diode and the $p-n$ junction is the critical structure

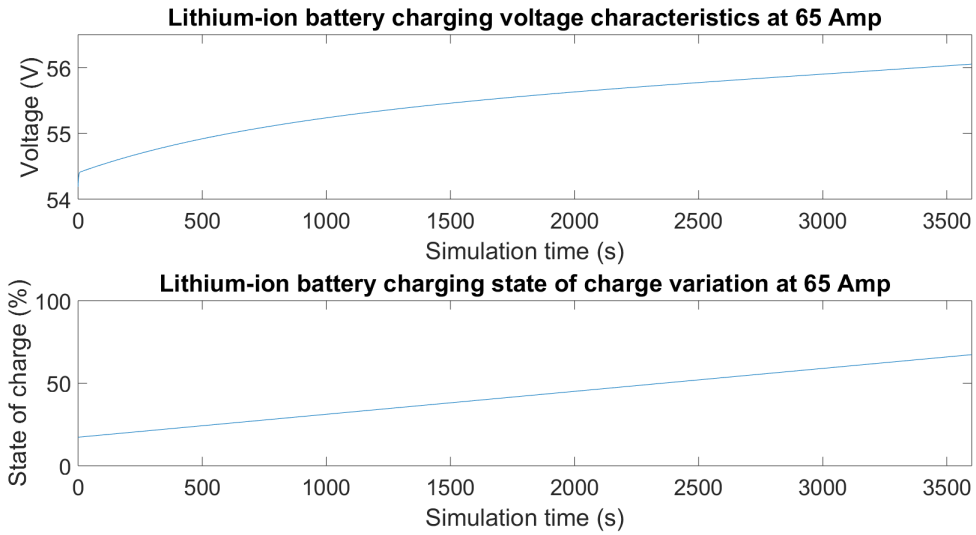

(a) Charging characteristics

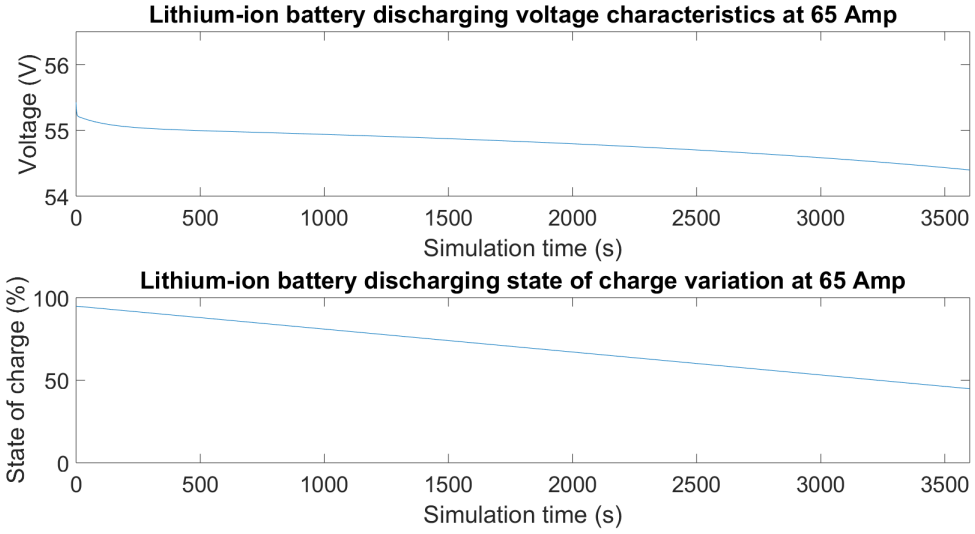

(b) Discharging characteristics

Fig. 2.9. Lithium ion battery charging and discharging characteristics

that can be triggered to generate current when exposed to sunlight. A $p-n$ junction is a boundary or interface between two types of semiconductor materials. The p side contains an excess of holes and the n side contains an excess of electrons. A single diode model of a PV cell (figure 2.11 [2]) was utilized in this study to obtain a

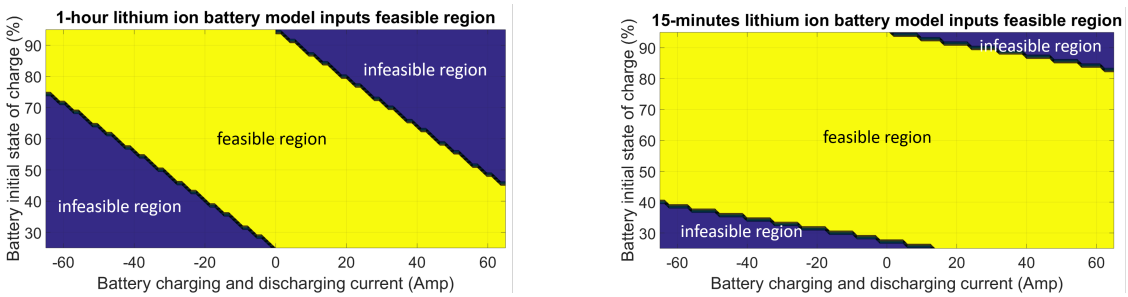

(a) 1 hour feasible region

(b) 15 minutes feasible region

Fig. 2.10. Lithium ion battery initial SOC and current feasible combination region

photovoltaic output power profile. I_{pv} is the current generated by the incident light, I_d is the Shockley diode equation 2.32, R_s is the equivalent series resistance of the array and R_p is the equivalent parallel resistance. The solution of the equation for this model leads to an $I - V$ relation for the PV cell that has the form in equation 2.33

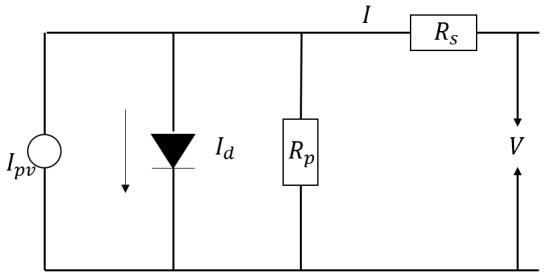

Fig. 2.11. schematic of single-diode model of PV cell

$$I_d = I_{0,cell}(e^{\frac{V_D}{V_t}} - 1) \tag{2.32}$$

where I_d is the diode current, $I_{0,cell}$ is the reverse saturation current, V_D is the voltage across the diode, V_t is the thermal voltage, i.e., $\frac{Akt}{q}$ (Boltzmann constant ($1.38906503\times 10^{-23}$) times temperature (in Kelvin) and A (ideality factor, typically varies from 1 to 2) divided by electron charge ($1.60217646 \times 10^{-19}$)).

$$I = I_{PV} - I_0[e^{\frac{V+R_sI}{N_sV_t}} - 1] - \frac{V + R_sI}{R_p} \tag{2.33}$$

where I_{PV} ($I_{PV} = I_{PV,cell}N_P$) is photovoltaic current of the photovoltaic array, I_0 ($I_0 = I_{0,cell}N_P$) is the saturation current of the photovoltaic array, V_t ($V_t = \frac{AkT}{q}$) is the thermal voltage, N_p is the number of cells connected in parallel to increase output current and N_s is number of cells connected in series to give the desired output voltage. Equation 2.33 results in an $I - V$ curve (figure 2.12) which represents characteristics of a PV panel. Three remarkable points in $I - V$ curve are the short circuit $(0, I_{sc})$, maximum power(V_{mp}, I_{mp}) and open circuit points $(V_{oc}, 0)$ [2].

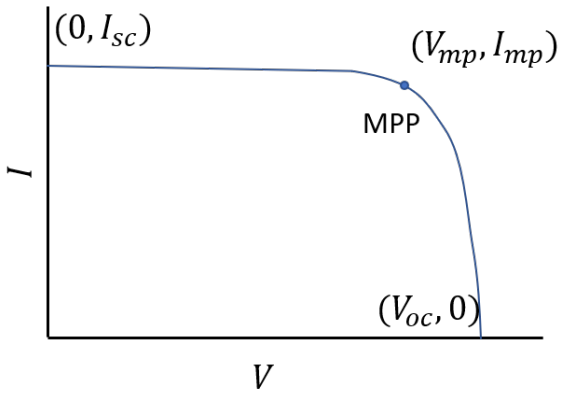

Fig. 2.12. Characteristic I-V curve of a PV cell

There are five unknowns in equation 2.33 which are I_{PV}, I_0, R_s, R_p and A to be determined in order to obtain an $I - V$ relation. For parameters R_s,R_p and A, an approach that refers to the manufactures' datasheet was utilized to compute them. Typically, the parameters provided from the data sheet are listed in table 2.5. The standard test condition means an irradiation of $1000W/m^2$ with an AM1.5 spectrum at 25°C, where AM1.5 means that air mass coefficient is 1.5 (The air mass coefficient defines the direct optical path length through the Earth's atmosphere, expressed as a ratio relative to the path length vertically upwards, i.e. at the zenith).

Table 2.5.
Parameters in datasheet

Parameters	
I_{sc}	short-circuit current in standard test conditions (STC)
V_{oc}	open-circuit voltage in STC
V_{mpp}	voltage at the Maximum Power Point (MPP) in STC
I_{mpp}	current at the MPP in STC
P_{mpp}	power at the MPP in STC
k_i	temperature coefficient of the short-circuit current
k_v	temperature coefficient of the open-circuit voltage

By substituting data for current and voltage at the three known points (the short-circuit, maximum power and the open-circuit points) into the $I-V$ equation, then the following three equations result [2].

$$\begin{aligned} I_{sc} &= I_{PV} - I_0 e^{\frac{I_{sc}R_s}{n_s V_t}} - \frac{I_{sc}R_s}{R_p} \\ I_{mpp} &= I_{PV} - I_0 e^{\frac{v_{mpp}+I_{mpp}R_s}{n_s V_t}} - \frac{V_{mpp}+I_{mpp}R_s}{R_p} \\ I_{oc} &= 0 = I_{PV} - I_0 e^{\frac{V_{oc}}{n_s V_t}} - \frac{V_{oc}}{R_p} \end{aligned} \tag{2.34}$$

Additional equations can be derived from maximum power point, where the derivative of power against voltage is zero, and also the derivative of the current against voltage at the short-circuit point [2].

$$\begin{aligned} \frac{dP}{dV}\Big|_{\substack{V=V_{mpp} \\ I=I_{mpp}}} &= 0 \\ \frac{dI}{dV}\Big|_{I=I_{sc}} &= -\frac{1}{R_s} \end{aligned} \tag{2.35}$$

From equations 2.34 and equations 2.35, theoretically $I_{PV,n}$, $I_{0,n}$, R_s, R_p and A can be solved numerically based on the manufactures' datasheet at standard test conditions (STC), where the subscript n denotes STC. In this study this method was adapted

such that only R_s, R_p and A were solved numerically, whereas $I_{PV,n}$, $I_{0,n}$ were obtained approximately by approaches shown below.

For I_{PV}, the photovoltaic current depends linearly on the solar irradiation and is also influenced by the temperature according to the following equation 2.36:

$$I_{PV} = (I_{PV,n} + k_i \delta_T) \frac{G}{G_n} \tag{2.36}$$

where $I_{PV,n}$ is the photovoltaic current at the standard test condition, k_i is temperature coefficient of the short-circuit current, $\delta T = T - T_n$ (in Kelvin) where T is the PV cell temperature and n denotes STC, G (watts per square meters) is the irradiation on the device surface, and G_n is the nominal irradiation. An assumption that $I_{sc,n} \approx I_{PV,n}$ is made because the series resistance of the single diode model is low and the parallel resistance is high. In summary, I_{PV} can be represented by equation 2.37, where all of the parameters can be obtained from data sheet values and from measurements.

$$I_{PV} = (I_{sc,n} + k_i \delta_T) \frac{G}{G_n} \tag{2.37}$$

For I_0, the diode saturation current and its dependence on the temperature can be expressed as equation 2.38:

$$I_0 = I_{0,n} (\frac{T}{T_n})^3 exp[\frac{qE_g}{Ak}(\frac{1}{T_n} - \frac{1}{T})] \tag{2.38}$$

where E_g is the bandgap energy of the semiconductor ($E_g = 1.12eV$ for the polycrystalline Si at 25°C) and $I_{0,n}$ is the nominal saturation current at the standard test conditions (STC), which could be expressed as follows:

$$I_{0,n} = \frac{I_{sc,n}}{exp(\frac{V_{oc,n}}{AV_{t,n}}) - 1} \tag{2.39}$$

where $V_{t,n}$ is the thermal voltage at the standard test condition.

The PV panel model selected for this study is model KC200GT [3]. The geometric specifications of a single PV panel are 1425mm(56.2in)× 990mm(39.0in) which is comprised of 54 PV cells. The other detailed specifications available in the manufactures' datasheet to retrieve a single diode PV cell model are listed in table 2.6.

Table 2.6.
KG200GT PV panel specifications

Electrical performance under standard test conditions	
Maximum Power (P_{mpp})	200W(+10% -5%)
Maximum Power Voltage (V_{mpp})	26.3V
Maximum Power Current (I_{mpp})	7.61A
Open Circuit Voltage (V_{oc})	32.9V
Short Circuit Current (I_{sc})	8.21A
Max System Voltage	600V
Temperature Coefficient of V_{oc}	-1.23×$10^{-1}V/°C$
Temperature Coefficient of I_{sc}	3.18×$10^{-3}A/°C$
Cells	
Number per Module	54
Physical specifications	
Length× Width× Depth	1425mm(56.2in)× 990mm(39.0in)× 36mm(1.4in)

Three important parameters (R_s,R_p and A) can be computed according to equations 2.34 and 2.35 based on required parameters in datasheet 2.6. The results are $R_s = 0.3625\Omega$, $R_p = 6928\Omega$ and $A = 1.0565$.

The predicted electrical characteristics using the single diode PV cell model are shown in figure 2.13 and the experimental data is shown by circles. From comparisons of the results, the single diode model of PV cell model constructed according to datasheet agrees well with the experimental data.

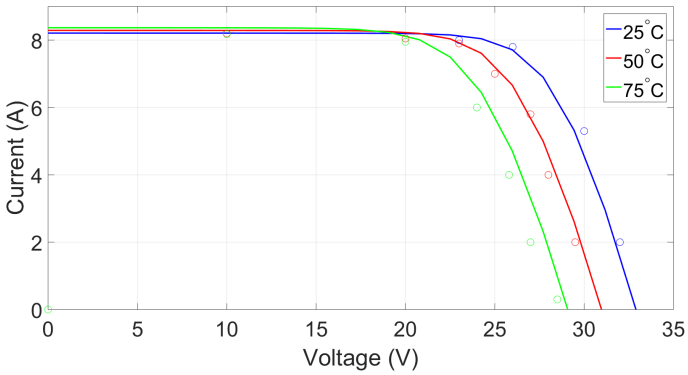

(a) Irradiance: AM1.5,1000W/m^2

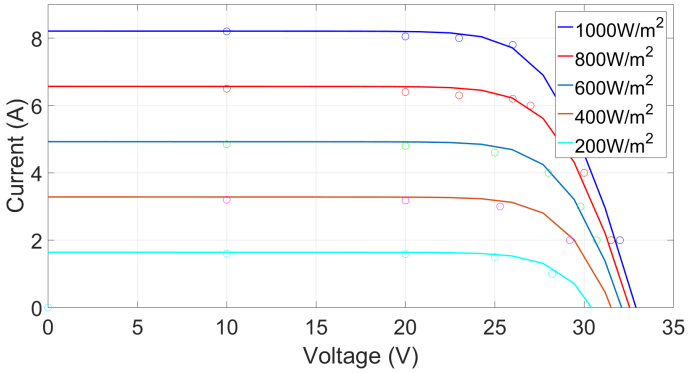

(b) Cell temperature: 25°C

Fig. 2.13. I-V characteristics of PV module KC200GT prediction

3. MODEL PREDICTIVE CONTROL

This chapter presents a global optimization approach, i.e., Dynamic Programming (DP), that searches for an optimal solution that minimizes monthly utility bills for the ice storage and battery systems. Both time-of-use energy (TOU) and demand charges are considered in the optimization problem. A typical optimization problem formulation using the concept of a demand target to handle a trade off between TOU energy costs and demand charges is developed first. Then a reformulated demand target reset algorithm that treats the demand target as an optimization constraint to only minimize energy cost is presented, which can tremendously reduce computational effort. This fast numerical approach not only improves practical MPC application speed but also allows annual economic performance analysis within a short simulation time.

3.1 Model predictive control formulation

The goal of this study is to compare economic performance of different systems under optimal control, therefore the controller doesn't consider model uncertainties and unmeasured disturbances. An idealized MPC was developed for evaluation purposes which assumes a perfect observer and no uncertainties in the model and load prediction.

3.1.1 Ice storage and photovoltaic system model predictive control

In the MPC formulation, it is assumed that chilled water supply temperature to the load is fixed at 44°F. The objective of MPC is to determine the sequences of control inputs which are chiller modes M and chiller outlet setpoints $T_{CHe,SP}$ for the

purpose of minimizing monthly utility bills. For the ice storage system, there are totally five modes which naturally result in a mixed integer nonlinear programming (MINLP) problem. Though MINLP can be used for analysis purposes, it is not preferred for MPC implementation. This is because there is a lack of freely available MINLP solvers and a MINLP-based MPC might be difficult to implement in an on-line solution since it may incur great computational effort such that it cannot be solved within the sampling time. In addition it is hard to consider demand charges because of a limited prediction horizon which is imposed by prediction errors and computational issues.

In order to deal with the first issue, an approach that maps ice storage capacity into plant modes was developed that converts the original mixed integer nonlinear programming (MINLP) problem into a nonlinear programming (NP) problem. For the second issue, an innovative reformulation of the original optimization problem minimizes time-of-use energy cost treating the demand charge as an adjustable constraint. If feasible solutions can not be found, a hard demand target is increased to the point where a feasible solution is found.

With the ice storage cooling capacity (discharge rate) as an optimization variable, the reformulated MPC problem is shown below [27]:

$$
\begin{aligned}
&\min_{z,u(0),\ldots,u(N-1)} \sum_{k=0}^{N-1} E(k)(P_{HVAC}(k)\Delta t - P_{solar}(k)\Delta t) + \omega \times z \\
&x_s(k+1) = x_s(k) - \frac{u(k)\Delta t}{C_s} \\
&0 \le Q_{CH}(k) \le Q_{CH,max}(T_{CH,i}(k), \dot{m}_{CH,i}(k), T_{OA}(k), maxstage) \\
&\begin{cases} u(k) \le Q_{IS,max,D}(T_{CH,e,SP}(k), \dot{m}_{CH,i}(k), x(k)) \quad if \quad (u(k) \ge 0) \\ -u(k) \le Q_{IS,max,C}(T_{CH,e,SP}(k), \dot{m}_{CH,i}(k), x(k)) \quad if \quad (u(k) < 0) \end{cases} \\
&Q_{CH}(k) = Q_{BL}(k) - u(k) \\
&T_{CHe,SP}(k) = \begin{cases} T_{CH,i}(k) - \frac{Q_{CH}(k)}{\dot{m}_{CH,i}(k) C_{p,w}} \quad if \quad (u(k) \ge 0) \\ 0 + \frac{u(k)}{\epsilon_C(\dot{m}_{CH,i}(k), x(k)) \dot{m}_{CH,i} C_{p,w}} \quad if \quad (u(k) < 0) \end{cases} \\
&T_{CH,i}(k) = T_{CHWS,SP}(k) + \frac{Q_{BL}(k)}{\dot{m}_{CH,i}(k) C_{p,w}} \\
&P_{HVAC}(k) = \begin{cases} 0 \quad if \quad (u(k) = 0, Q_{BL} = 0) \\ P_{CH}(Q_{CH}(k), T_{CH,e,SP}(k), T_{OA}(k)) + P_{pump}(\dot{m}_{CH,i}) \quad (otherwise) \end{cases} \\
&D(k)(P_{HVAC}(k) + P_{non-HVAC}(k) - P_{solar}(k)) \le z \quad (k \in \{0, \ldots, N-1\}) \\
&x_{s,l} \le x_s(k) \le x_{s,u}
\end{aligned}
\tag{3.1}
$$

where, $E(\$/kWh)$ is time-of-use energy cost and $D(\$/kW)$ is demand charge. P_{HVAC} is the electric power associated with the HVAC system and $P_{non-HVAC}$ is the electric power excluding HVAC power. P_{solar} is the total PV panel generation rate. N is a look-ahead horizon which ideally should cover a billing period (one month). z is a demand limit which is also to be optimized and ω is a weighting number introduced to compensate for the reduced time period if N is less than the billing period. u is control input to be optimized which is the ice storage cooling capacity (discharge rate) in the formulation. Variables required to be predicted are T_{OA} and Q_{BL}, which are assumed

perfect predictions in this study. The variables of $T_{CH,i}, \dot{m}_{CH,i}, Q_{CH}$ and $T_{CHe,SP}$ are internal variables to be calculated for the chiller and ice-storage components.

The first constraint represents the ice storage dynamics using the concept of state of charge (SOC). The first inequality denotes the chiller capacity range at time step k. The second and third inequalities state capacity limits for the ice storage tank during discharging and charging processes at time step k. The equation for Q_{CH} specifies the cooling load left for the chiller after subtracting the ice storage capacity from the total building cooling load. The equation for $T_{CHe,SP}$ is switched depending on the ice-storage modes, where the first equation for the discharging process is simply an energy balance for the chiller and the second equation for the charging process is from the ϵ -NTU relation for the ice storage. The HVAC power includes chiller and pump power. If there is no building cooling load, and ice tanks are not charged, the HVAC power is set to 0. The second last inequality denotes the demand limit constraint, and the last inequality specifies ice storage state of charge constraints ($x_{s,l} = 0$ and $x_{s,u} = 1$).

Even though the reformulation converts the original MINLP problem into a more tractable NP problem, many NP algorithms would still fail to solve it because the functions that describe capacity constraints and power are discontinuous due to the discrete nature of the operating mode. Therefore, a gradient-based optimization approach cannot be used. Besides, gradient-free algorithms such as the genetic algorithm(GA), are typically not applicable for on-line MPC implementation because of computational requirements and there is no guarantee of a global optimal point.

3.1.2 Battery and photovoltaic system model predictive control

For the battery system integrated with photovoltaics, the cooling plant only has "chiller-only" and "off" modes. For this system the chiller cooling capacity should be sufficient to meet the peak building load. Similar to an ice storage system, the

battery charging (or discharging) current rate is an optimization variable and the MPC problem was formulated as below:

$$
\begin{aligned}
&\min_{z,I(0),\ldots,I(N-1)} \sum_{k=0}^{N-1} E(k)(P_{HVAC}(k)\Delta t - P_{solar}(k)\Delta t + P_b(k)\Delta t) + \omega \times z \\
&x_b(k+1) = x_b(k) + \frac{I(k)\Delta t}{Q_{bat,I}} \\
&0 \le Q_{CH}(k) \le Q_{CH,max}(T_{CH,i}(k), \dot{m}_{CH,i}(k), T_{OA}(k), maxstage) \\
&Q_{CH}(k) = Q_{BL}(k) \\
&T_{CHe,SP}(k) = T_{CHWS,SP}(k) \\
&T_{CH,i}(k) = T_{CHWS,SP}(k) + \frac{Q_{BL}(k)}{\dot{m}_{CH,i}(k) C_{p,w}} \\
&P_{HVAC}(k) = \begin{cases} 0 \quad if \quad (Q_{BL} = 0) \\ P_{CH}(Q_{CH}(k), T_{CH,e,SP}(k), T_{OA}(k)) + P_{pump}(\dot{m}_{CH,i}) \quad (otherwise) \end{cases} \\
&D(k)(P_{HVAC}(k) + P_{non-HVAC}(k) - P_{solar}(k) + P_b(k)) \le z \quad (k \in \{0, \ldots, N-1\}) \\
&P_b(k) = F(I(k), x_b(k), \Delta t) \\
&x_{b,l} \le x_b(k) \le x_{b,u}
\end{aligned}
\tag{3.2}
$$

where I is the battery current (charging is positive and discharging is negative), P_b is the battery charging (or discharging) rate (kW) as a function of current (I), initial state of charge (x) and time step (Δt), and $Q_{bat,I}$ is the battery capacity (Amp-hours). The battery's state of charge is constrained between 25% and 95% to avoid deep depletion and over-charging.

3.2 Global optimization through dynamic programming algorithm

3.2.1 Basic Problem

For a deterministic discrete-time dynamic system:

$$
x_{k+1} = f_k(x_k, u_k), \qquad k = 0, 1, \ldots, N-1 \tag{3.3}
$$

where the state x_k is an element of a space S_k and the control u_k is an element of a space C_k. The control u_k is constrained to take values in a given nonempty subset $U(x_k) \subseteq C_k$, which depends on the current state x_k, i.e., $u_k \in U_k(x_k)$ for all $x_k \in S_k$ and k [28].

The class of policies that consist of a sequence of functions:

$$\pi = \{\mu_0, \ldots, \mu_{N-1}\} \tag{3.4}$$

where μ_k maps states x_k into controls $u_k = \mu_k(x_k)$ and is such that $\mu_k(x_k) \in U_k(x_k)$ for all $x_k \in S_k$. Such policies will be called admissible. Given an initial state x_0 and an admissible policy $\pi = \{\mu_0, \ldots, \mu_{N-1}\}$, the system equation can be defined as follows:

$$x_{k+1} = f_k(x_k, \mu_k(x_k)), \qquad k = 0, 1, \ldots, N-1 \tag{3.5}$$

For given functions g_k, $k = 0, 1, \ldots, N$, the cost of policy π starting at x_0 is:

$$J_\pi(x_0) = \sum_{k=0}^{N-1} g_k(x_k, \mu_k(x_k), w_k) + g_N(x_N) \tag{3.6}$$

where $g_N(x_N)$ is the terminal cost. An optimal policy π^* that minimizes cost function 3.6 for a given initial state x_0 satisfies the following equation:

$$J_{\pi^*}(x_0) = \min_{\pi \in \Pi} J_\pi(x_0) \tag{3.7}$$

where π is the set of all admissible policies. Hence J_{π^*} is a function of initial state x_0 which is called the optimal cost function.

3.2.2 Dynamic programming algorithm

Principle of Optimality

The dynamic programming algorithm relies on the principle of optimality. Let $\pi^* = \{\mu_0^*, \mu_1^*, \ldots, \mu_{N-1}^*\}$ be an optimal policy for the basic problem (deterministic

problem). Consider the subproblem whereby we are at x_i at time i and wish to minimize the cost function from time i to time N:

$$\sum_{k=i}^{N-1} g_k(x_k, \mu_k(x_k), w_k) + g_N(x_N) \tag{3.8}$$

Then the truncated policy $\{\mu_i^*, \mu_{i+1}^*, \ldots, \mu_{N-1}^*\}$ is optimal for this subproblem.

Backward dynamic programming algorithm

The optimization problem and principle of optimality are combined to give a dynamic programming algorithm as follows:

For every initial state x_0, the optimal cost $J^*(x_0)$ of the basic problem is equal to $J_0(x_0)$, given by the last step of the following algorithm, which proceeds backward in time from period $N-1$ to period 0:

$$J_N(x_N) = g_N(x_N) \tag{3.9}$$

$$J_k(x_k) = \min_{u_k \in U_k(x_k)} g_k(x_k, u_k) + J_{k+1}(f_k(x_k, u_k)) \quad k = 0, 1, \ldots, N-1 \tag{3.10}$$

Then the optimal cost is $J_0(x_0)$ (also called the shortest path). Furthermore, if $u_k^* = \mu_k^*(x_k)$ minimizes the right side of equation 3.10 for each x_k and k, the policy $\pi^* = \{\mu_0^*, \ldots, \mu_{N-1}^*\}$ is optimal. This leads to an important property of deterministic problems that minimizing the cost over admissible policies $\{\mu_0, \ldots, \mu_{N-1}\}$ results in the same optimal cost as minimizing over sequences of control vectors $\{u_0, \ldots, u_{N-1}\}$. This is true because for given a policy $\{\mu_0, \ldots, \mu_{N-1}\}$ and initial state x_0, the future states are perfectly predictable through the equation:

$$x_{k+1} = f_k(x_k, \mu_k(x_k)) \quad k = 0, 1, \ldots, N-1 \tag{3.11}$$

and the corresponding controls are perfectly predictable through the equation:

$$u_k = \mu_k(x_k) \quad k = 0, 1, \ldots, N-1 \tag{3.12}$$

Thus, the cost achieved by an admissible policy $\{\mu_0, \ldots, \mu_{N-1}\}$ for a deterministic problem is also achieved by the control sequence $\{u_0, \ldots, u_{N-1}\}$ defined above. For

the deterministic problem, we restrict our attention to sequences of controls. Though analytical expressions for a control sequence $\{u_0, \ldots, u_{N-1}\}$ are not possible, a numerical table can store sequences of controls to be used further.

Parametric cost approximation

In an ice storage system, though there is only one state variable and one control variable, but both are continuous. The problem is simplified by discretizing both the state and control variables. Consider discretization and piecewise linear approximation for the ice storage case where the state of charge is an interval $[0, 1]$. Consider a set of grid points $\{d_0, \ldots, d_n\}$ within $[0, 1]$, which includes the endpoints a and b, and is viewed as the set of aggregate states. In this study, n was chosen as 20 which means we have total 21 discrete points to approximate the entire continuous state of charge range. The same approach is applied to the control space, in which case the total discrete grid point number is 51. For any nongrid point $x \in [a, b]$, the cost approximation $\tilde{J}_k(x)$ is obtainted by linear interpolation of the costs of the two grid points $\underline{d}(x)$ and $\bar{d}(x)$ that are adjacent to x from above and below:

$$\tilde{J}_k(x) = \frac{\bar{d}(x) - x}{\bar{d}(x) - \underline{d}(x)} r_{\underline{d}(x)} + \frac{x - \underline{d}(x)}{\bar{d}(x) - \underline{d}(x)} r_{\bar{d}(x)} \tag{3.13}$$

where $r_{\underline{d}(x)}$ and $r_{\bar{d}(x)}$ are the optimal cost of $\underline{d}(x)$ and $\bar{d}(x)$ in the aggregate problem, whose states are the grid points $\{d_0, d_1, \ldots, d_n\}$. There exists a trade-off between accuracy of this approximation and computational speed with respect to the number of grid points.

3.3 Demand limit reset strategy

A natural objective function of an MPC is to minimize the time-of-use energy cost and demand charge simultaneously while meeting building loads and equipment capacity constraints. Hence, it can be represented in a condensed way:

$$\min_{u(0),\ldots,u(N-1)\in U} \sum_{k=0}^{N-1} E(k)P_t(k)\Delta t + max(D(k)(P_t(k)+P_{non-HVAC}(k)|k \in \{0,\ldots,N-1\}) \tag{3.14}$$

where P_t for an ice storage system is $P_{HVAC}(k) - P_{solar}(k)$ and for a battery system is $P_{HVAC}(k) - P_{solar}(k) + P_b(k)$. U represents a feasible set imposed by dynamics, equality and inequality constraints. In the MPC, time-of-use energy costs are also assumed to be charged based on 1 hour average power same as the demand costs. Ideally, N should cover a billing period which is one month. However, it is not practical to consider an entire monthly time horizon because of computational requirements and prediction uncertainties of disturbances such as outdoor temperature and occupancy.

In order to reduce computation, it is popular to convert problem 3.14 into a more numerically friendly form which is shown below [10]:

$$\begin{aligned} \min_{z,u(0),\ldots,u(N-1)\in U} \quad & \sum_{k=0}^{N-1} E(k)P_t(k)\Delta t + \omega \times z \\ \text{s.t.} \quad & D(k) \times (P_t(k) + P_{non-HVAC}(k)) \leq z \quad \forall k \in \{0,\ldots,N-1\} \end{aligned} \tag{3.15}$$

where $z \in R$ is an additional variable to be optimized. The additional inequality constraint denotes that z is an upper bound of a demand charge in the prediction horizon. Therefore this reformulated problem can minimize the time-of-use energy cost and demand charge simultaneously. If the weight factor ω is 1, then problem 3.14 and problem 3.15 are equivalent which means the optimal point of the latter solves the former and optimal costs are the same. A typical MPC strategy to consider a demand charge in the literature is to set N to a reduced prediction horizon, e.g., one day. In this case, the weight factor can be adjusted to compensate for the reduced time period. Kim [27] proposed an approach that reformulates the optimization problem

3.15 into 3.16 which only solves the time-of-use energy cost minimization problem with a demand limit constraint.

$$\begin{aligned} &\min_{u(0),\ldots,u(N-1)\in U} \quad \sum_{k=0}^{N-1} E(k)P_t(k)\Delta t \\ &\text{s.t.} \quad D(k) \times (P_t(k) + P_{non-HVAC}(k)) \leq \hat{z}_m^* \quad \forall k \in \{0,\ldots,N-1\} \end{aligned} \tag{3.16}$$

The final MPC algorithm proposed is shown below and a demand limit reset algorithm flow chart is shown in figure 3.1.

1) For the first sampling time of a billing period, initialize $\hat{z}_M^*$ as

$$\hat{z}_M^* = max\{D(k)P_{non-HVAC}(k)|k \in \{0,\ldots,N-1\}\}, \tag{3.17}$$

where $P_{non-HVAC}$ is the predicted power within a prediction horizon.

2) Solve the energy cost optimization problem 3.16.

3) If there exists a feasible solution, then maintain $\hat{z}_M^*$.

4) If there is no feasible solution, then increase $\hat{z}_M^*$ a little bit until a feasible solution could be found.

5) Feed the first part of optimal control inputs into the plant and repeat from step 2 to 4.

The MPC algorithm was implemented through dynamic programming that is computationally efficient. The following figures illustrate system responses determined by the MPC controller for both the ice storage and battery systems. It should be mentioned that all the components were not optimally sized. The goal here is to compare optimal control system response differences for systems with ice storage or batteries. Figure 3.2 illustrates the responses for a 75-ton central cooling plant coupled with a 330 ton-hour ice storage and a 40 kW PV array under the proposed MPC controller. The black dash line denotes the scaled on-peak, partial-peak and off peak electricity cost rates. For August 2nd, all of the HVAC load was shifted into the off-peak period. However there was a power peak for power purchased from the grid. In this case, this is the difference between non-HVAC load and PV generation rate. Even though in

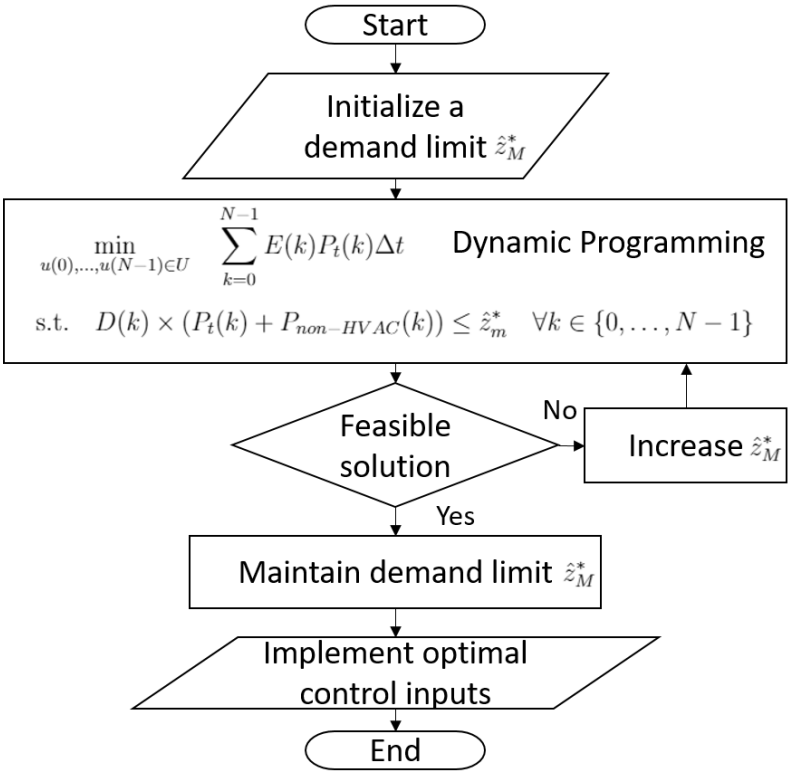

Fig. 3.1. MPC demand limit reset algorithm

commercial buildings non-HVAC load is pretty flat and stable, after integration with renewable energy resources, e.g., PV, there could still be power peaks for purchasing electricity. Figure 3.3 shows the responses of a 75-ton central cooling plant coupled with a 0.5 C-rate 385 kWh lithium-ion battery bank and a 40 kW PV array under MPC. The battery size was determined to be similar to the ice storage size considering the COP. It could be observed that batteries respond to the total building load peak by releasing more energy such that the net power purchased from the utility grid doesn't have a power spike. This is due to the flexibility of batteries that can shift both HVAC and non-HVAC loads as compared to a case of the ice storage system. Hence, batteries are more effective for shaving peak power when a system is coupled with PV.

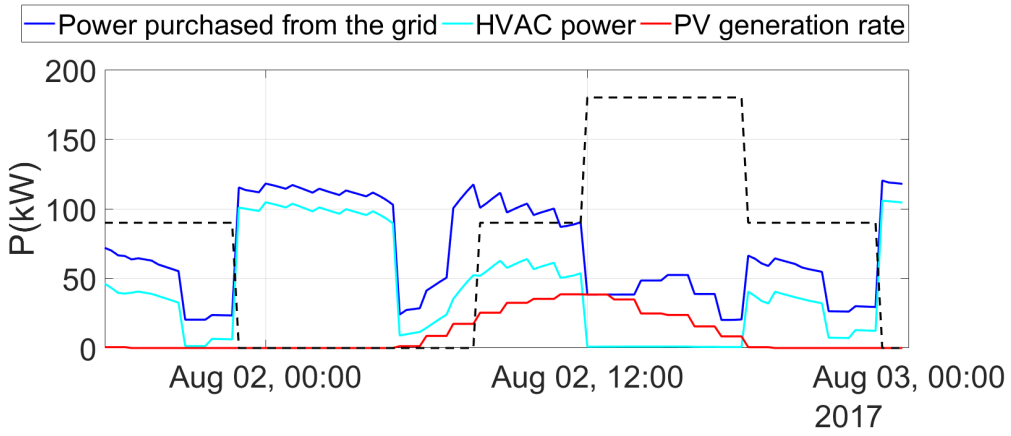

Fig. 3.2. Responses of system coupled with ice storage and PV under MPC controller

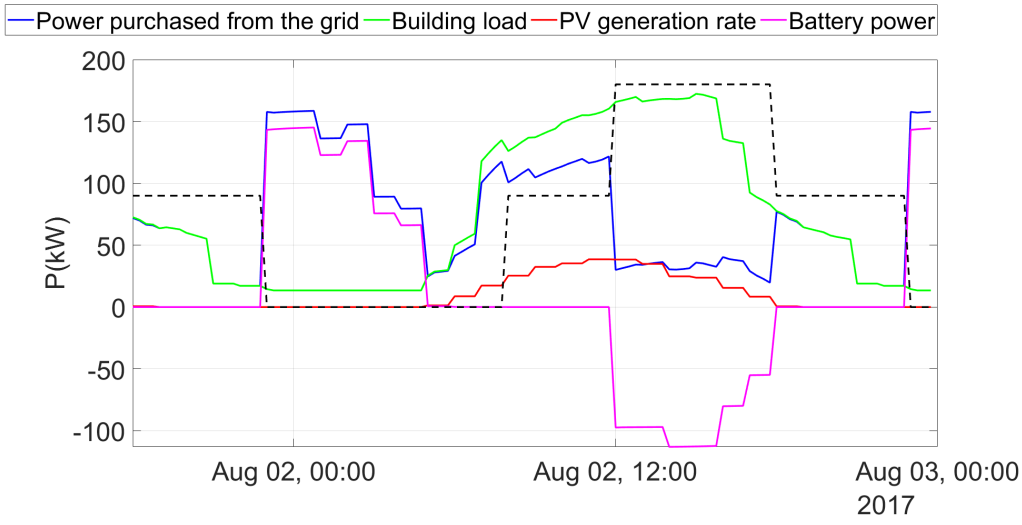

Fig. 3.3. Responses of system coupled with batteries and PV under MPC controller

4. OPTIMAL SYSTEM COMPONENT SIZING AND SYSTEM COMPARISONS

This chapter presents approaches for chiller, ice storage, battery and photovaltics array optimal size determination in terms of life cycle costs. In order to compare different systems fairly, one that uses thermal storage and another that uses batteries, the sizes of components in each system to be considered play a crucial role. In this chapter, optimal size strategies for each system in terms of life cycle costs were developed for the purpose of comparing the best designs for each system. By combining optimal sizing with a model predictive control algorithm, comparisons between systems coupled with thermal storage or batteries were carried out in the fairest way thought possible.

4.1 Chiller and ice storage optimal size determinations

The approach of determining the optimal size of a thermal storage system depends on utility rate structure such as the "on-peak" and "off-peak" energy cost ratio, demand charge, the initial cost of each component, and the building load profiles. Two general and popular sizing strategies for ice storage systems are full storage and partial storage.

In a full storage system, the storage capacity should provide all cooling loads during on-peak hours and the chiller is employed only in off-peak hours. This type of sizing leads to relatively large storage and chillers. A typical operation scheme is shown in figure 4.1(a). The building load during on-peak hours is met by the ice storage releasing its stored cooling energy. During off-peak hours, the chiller uses its full capacity to charge the ice storage and can also provide some building cooling

when needed. All the building cooling is provided eventually by the chiller, so that the integrated load on the chiller equals the integrated building load.

In a partial storage system, the chiller runs continuously on the design day and the ice storage provides the remaining cooling not met by the chiller. A typical operation scheme is shown in figure 4.1(b), where the chiller capacity in charging and cooling modes is relatively constant depending on the chiller supply temperature and ambient conditions. The chiller is sized in order to meet the integrated building

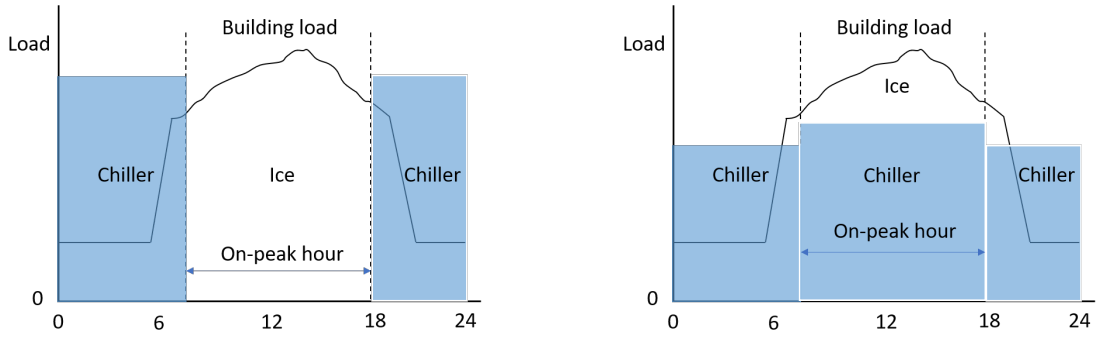

(a) Full storage

(b) Partial storage

Fig. 4.1. Schematic of design-day operations of the ice storage

load while operating continuously at maximum capacity over the entire day. The chiller capacity during the ice making mode is less than the on-peak period due to the low evaporating temperature when producing ice. The ice storage is sized to meet the difference between the load and chiller capacity during the on-peak period on the design day. This sizing approach tends to minimize the sizes of both the chiller and storage leading to minimum installed cost if storage is utilized. With a partial storage system, two common control strategies are used during the daytime: chiller priority and storage priority control. Chiller priority control has the chiller run with its maximum capacity and the storage meets the remaining load. Storage priority control has the storage meet the load first and the chiller meets the rest of the cooling load.

Full storage and partial storage sizing, though commonly employed, result in two extreme sets of sizing for the chiller and ice storage. There are many other size combinations of the chiller and ice storage between full storage and partial storage which might have better economic performance over these two conventional chiller and ice storage sizes in terms of life cycle costs.

4.1.1 Search region for chiller and storage size combinations

In order to evaluate life cycle costs for different size combinations of chiller and ice storage, the first step is to determine the feasible search region. Figure 4.2 shows the search region that was considered in this research. The horizontal and vertical

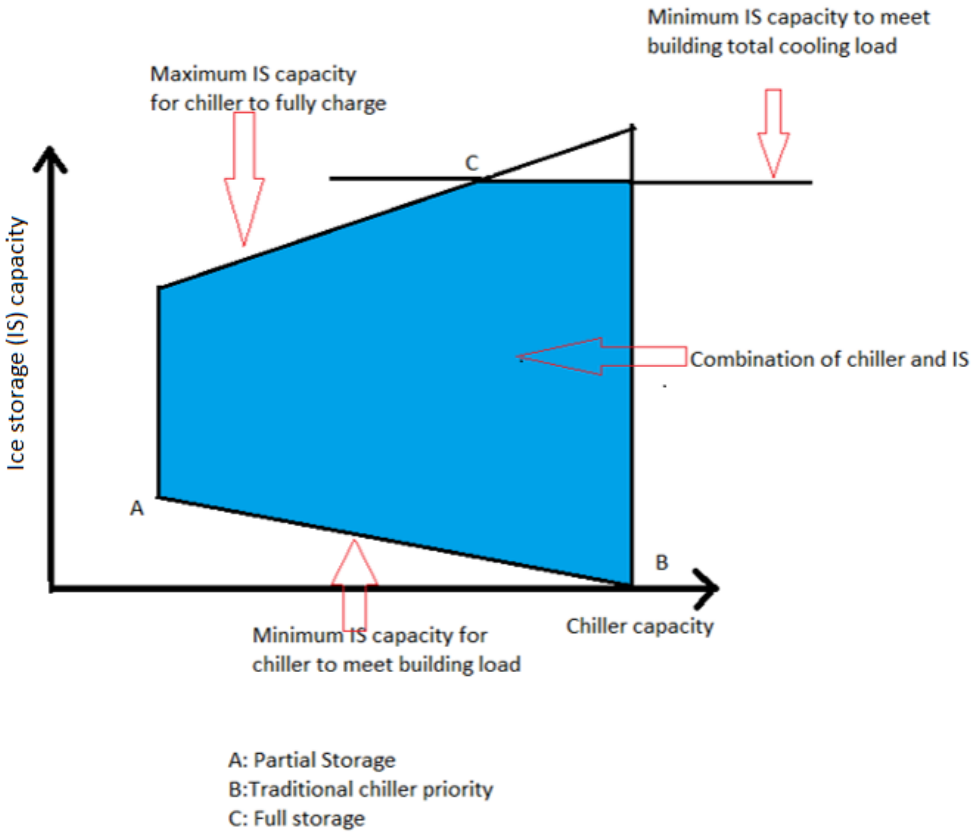

Fig. 4.2. schematic of the search region

axes denote the chiller capacity and ice storage capacity respectively. The point "A" is partial storage sizing that minimizes the chiller and ice storage sizes, and the associated installed costs when storage is utilized. Point "B" is a conventional system without storage that only uses the chiller to provide cooling throughout the day. Point "C" is a full storage system with maximum ice storage and chiller capacity. The bottom boundary of the search region is the minimum ice storage capacity as a function of chiller capacity such that they could meet the design day cooling load together. The minimum storage capacity decreases with increasing chiller capacity since with a greater chiller capacity the remaining cooling load to be met by ice storage is less. The upper boundary contains an inclined line and a horizontal line. The inclined line represents the maximum ice storage capacity that a given sized chiller could fully charge during unoccupied hours on the design day. The slope is upward since a greater chiller capacity can produce more ice. The horizontal line specifies the minimum ice storage capacity required to meet the on-peak building load by itself, beyond which the extra capacity is useless incurring some unnecessary initial costs. The intersection of these two lines at point C is the full storage design point where the ice storage capacity is sufficient to meet the on-peak building load and the chiller capacity is the minimum necessary to fully charge it during the unoccupied period. The left and right boundaries are both determined by the chiller capacity which specify the minimum and maximum chiller capacity, respectively.

Conventionally, points "A", "B" or "C" are used depending on cost considerations, utility rates, and control strategies. A rule of thumb is that the partial storage sizing has much better economics than the full storage and traditional HVAC system in terms of the life cycle cost when appropriate utility incentives are in place. The partial storage system can spread out building loads evenly throughout the day, and minimizes chiller and ice storage sizes. The full storage system has the highest investment cost which typically leads to greater life cycle cost than partial storage even though the operating costs are lower.

An intriguing question that naturally comes from the figure 4.2 is whether the partial storage system is the point having the minimum life cycle cost among the search region or not.

4.1.2 Life cycle cost graph

An optimal sizing strategy for the chiller and ice storage in terms of life cycle costs should employ optimal control for all possible size combinations within the search region (figure 4.2). In order to generate a life cycle cost graph over the search region, it is necessary to sample many points among the search region where each point is an annual simulation. This requires a significant computational effort because of implementation of an optimal control algorithm. The optimal control algorithm proposed in this study (equation 3.16) is computationally efficient so that life cycle costs for the sampled points within the search region could be computed in an acceptable period of time. The life cycle cost depends on both initial costs of components and operating costs, which depend on building type, climate zone and utility rates to be considered. This study addresses optimal chiller and storage sizes for the case study and utility rates described in chapter 2. The chiller and ice storage installed costs are taken to be 735 $/ton for the chiller and 126 $/ton-hour for the ice tank. Life cycle cost graphs for the three utility rate plans considered are shown in figure 4.3, 4.4 and 4.5.

4.1.3 Life cycle cost analysis

From the life cycle cost graphs and contours for the three utility rate plans, the minimum life cycle cost is near the minimum chiller and ice storage size. In addition, the variation in life-cycle costs near this point is pretty small. The life cycle cost magnitude and variation near the full storage and conventional HVAC systems are much higher than the region around the partial storage point.

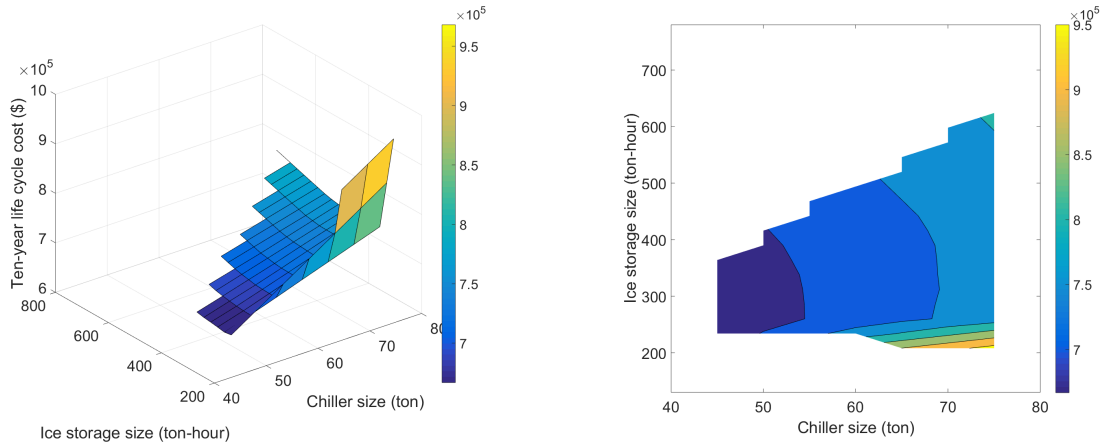

(a) Life cycle cost graph (b) Life cycle cost contour

Fig. 4.3. Utility rate A10 life cycle cost

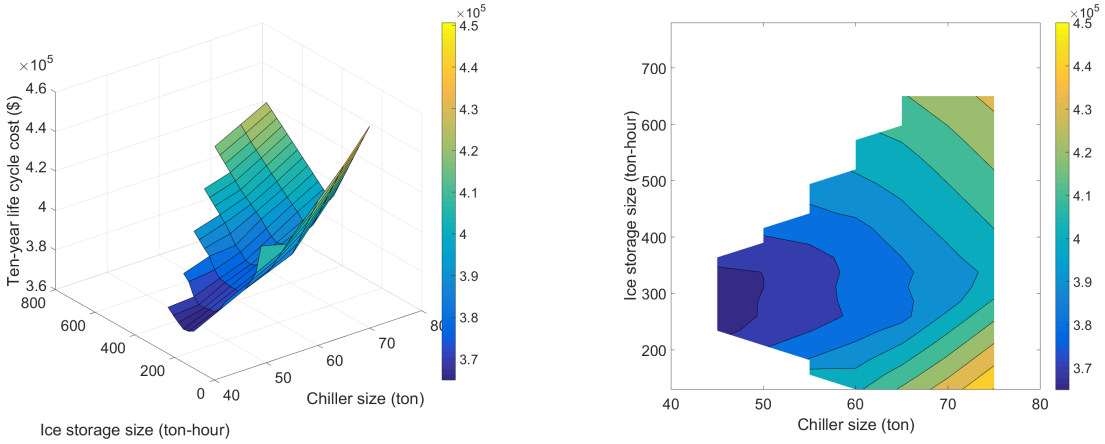

(a) Life cycle cost graph (b) Life cycle cost contour

Fig. 4.4. Utility rate GS-2B life cycle cost

Partial storage point definition

Conventionally, a chiller for a partial storage system charges ice storage with its full capacity during unoccupied periods as shown in figure 4.1(b), and the chiller and ice storage size are minimized. However, this minimum size ice storage tends to be charged near 100% state of charge (SOC) which results in a significant drop of

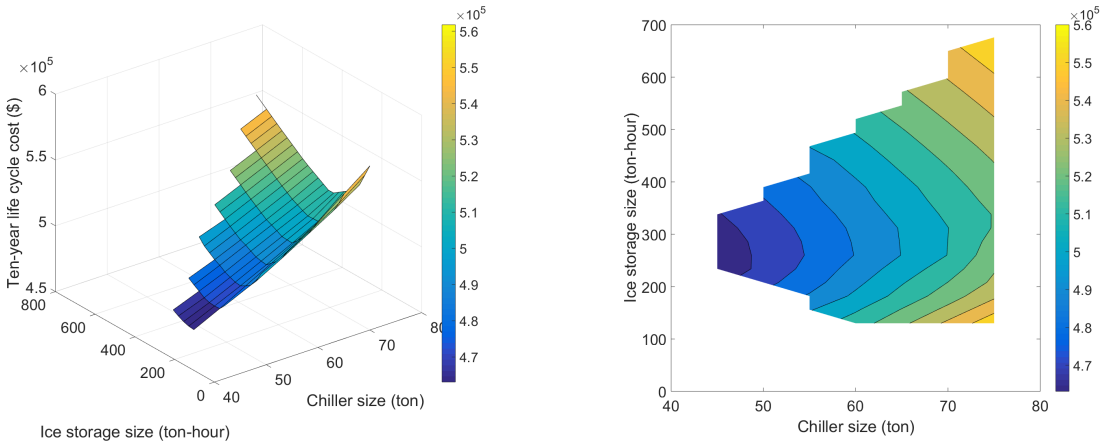

(a) Life cycle cost graph

(b) Life cycle cost contour

Fig. 4.5. Utility rate GS-R life cycle cost

heat transfer effectiveness. Figure 4.6 shows a significant drop in capacity when SOC exceeds about 95%(figure 4.6(a)) due to a drop in heat transfer effectiveness. This leads to less total cold energy stored in the ice storage. Therefore, during the occupied period ice storage could deliver less cold energy to the building such that the operating cost increases a little bit. The minimum life cycle cost point in figure 4.7 occurs when the chiller could charge ice storage at a relatively constant rate which is illustrated in figure 4.6(b). Slightly increasing ice storage capacity from the minimum size helps the chiller produce ice with a high heat transfer effectiveness resulting in a lower maximum SOC. This chiller charging performance coincides with the conventional partial storage definition. Similar results were found with the other utility rate plans. Therefore we define ice storage capacity of a partial storage system as the minimum capacity that the smallest possible chiller could charge with a relatively constant rate on the design day.

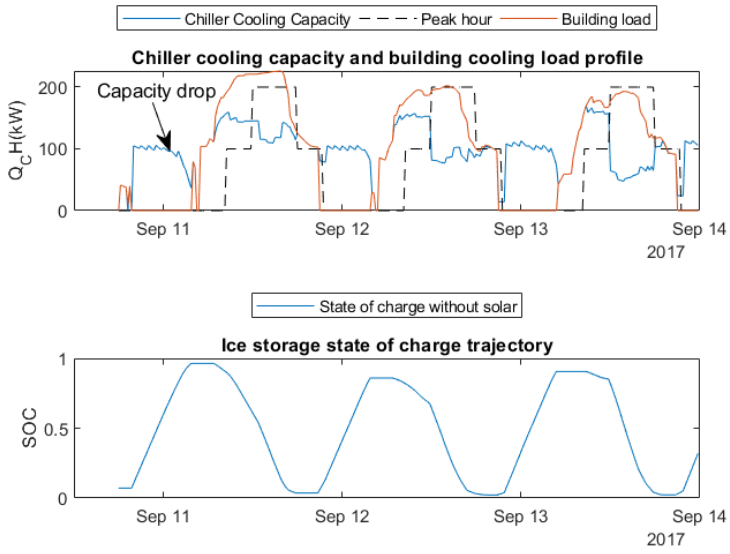

(a) 45 ton chiller with 234 ton-hour ice storage

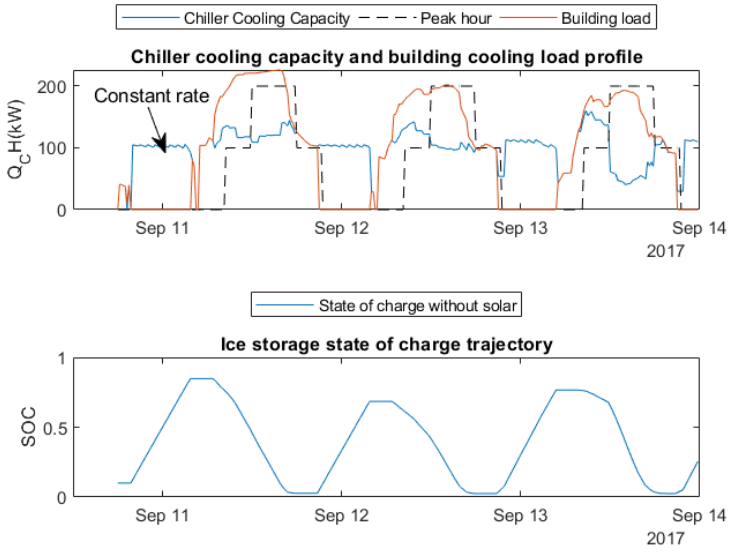

(b) 45 ton chiller with 312 ton-hour chiller

Fig. 4.6. Responses of chiller capacity and ice storage SOC

Life cycle cost sensitivity analysis

Even though the overall system life cycle cost graphs under utility rate A-10, GS-2B and GS-R have the same shape, they have different sensitivities to sizing. Figure

4.8 shows three normalized life cycle cost contours for the three utility plans (A10, GS-2B, GS-R). The size combination of 45 ton chiller and 312 ton-hour ice storage serves as the baseline for normalization.

We analyzed the size sensitivity along two directions that are shown in figure 4.8(a), one of which is from the minimum cost point to the full storage point and the other is to the conventional chiller point. All three utility rate plans have a TOU energy cost with a favorable on-peak to off-peak ratio. The difference is the demand charge schedule.

For the first direction, the overall sizing sensitivities for three utility rate plans are all small, which means increasing installed costs of chiller and ice storage compensate for the increasing operating cost savings with a larger ice storage capacity. For the second direction, the life cycle cost sensitivity of utility rate A10 is much higher than the others. This is because utility rate A10 has an any-time demand charge both in summer and winter. When ice storage capacity decreases, the operating costs coming from demand charges dramatically increase in all twelve months (cooling load exists even during winter utility rate period). On the contrary, utility rate GS-2B and utility rate GS-R don't have a demand charge in winter and therefore have a lower sensitivity to sizing near the optimum.

In summary, minimum life cycle cost points for all three utility rate plans are near the partial storage point and their life cycle cost sensitivities highly depend on demand charge rates and schedules.

4.2 Photovoltaic optimal sizing in combination with a central cooling system coupled with ice storage

In this section, two sizing strategies for PV combined with a central cooling system coupled with ice storage (figure 2.4) are proposed. The first one involves directly searching for the optimal PV size in terms of life cycle cost with the proposed MPC algorithm implemented for a prescribed partial storage system. The second method

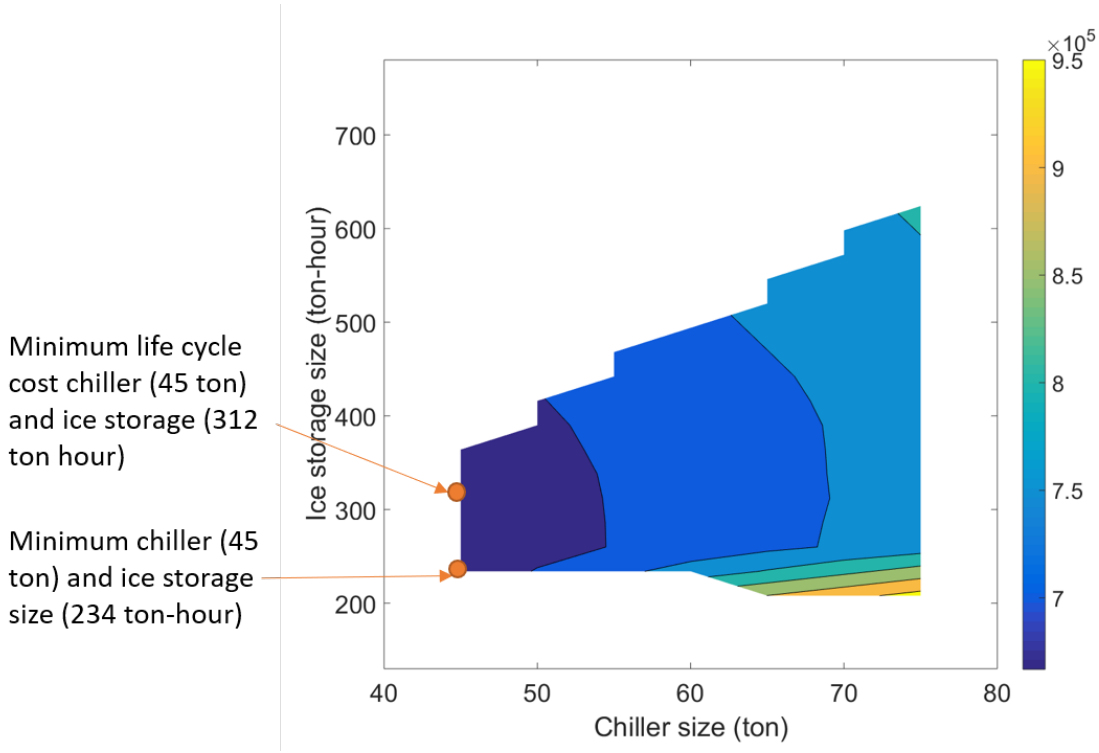

Fig. 4.7. Utility A10 life cycle cost contour

attempts to reduce the computational effort by decoupling the control and sizing processes. This sequential optimal sizing scheme is validated using the direct search method.

4.2.1 Optimization methodology

Optimal sizing in combination with MPC algorithm

The optimal sizes of chiller and ice storage are assumed to be the partial storage solution since the cost sensitivity around this region is small. With this prescribed central cooling plant size, the simplest method to size a PV system is to perform annual simulations with the proposed MPC algorithm for different PV sizes and find the size that minimizes the life cycle cost. This method is termed as direct search.

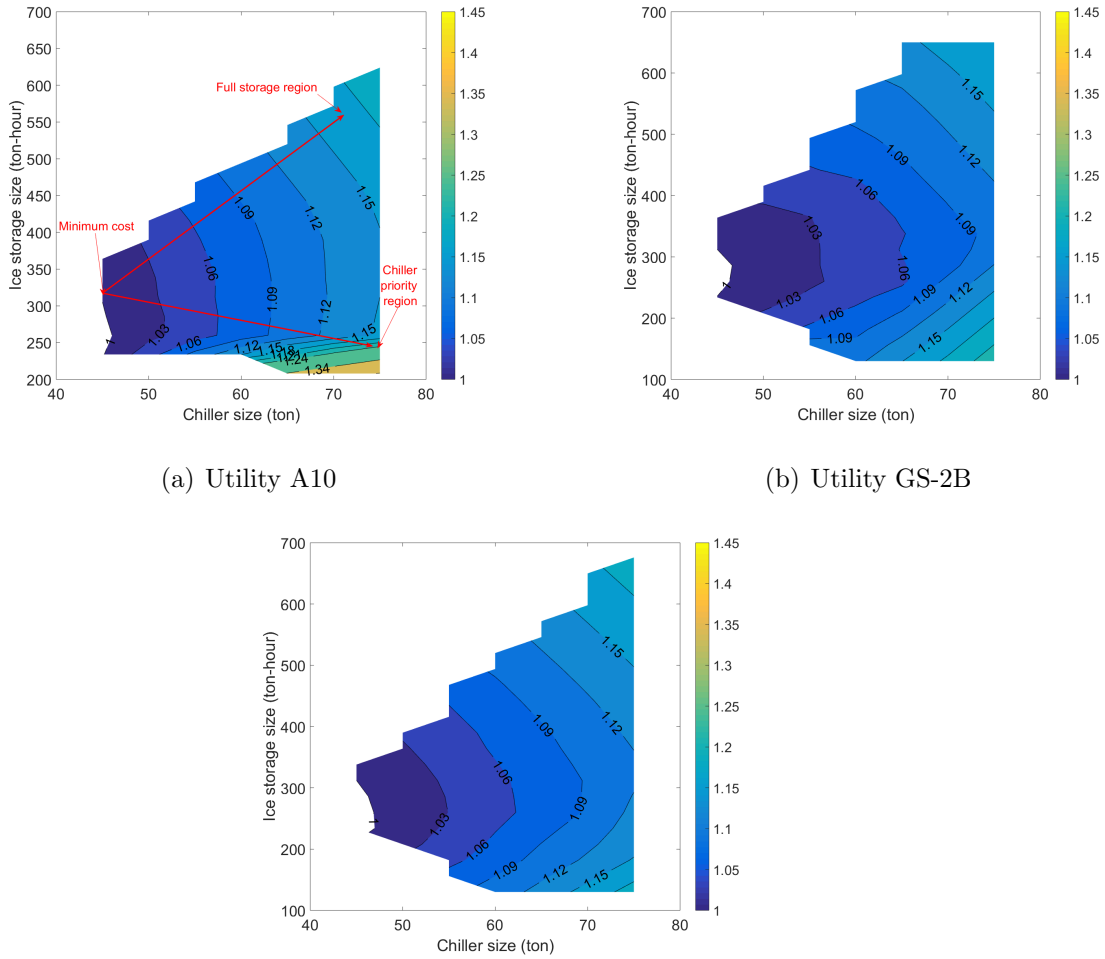

(a) Utility A10

(b) Utility GS-2B

(c) Utility GS-R

Fig. 4.8. Normalized life cycle cost contour

Sequential Optimization

The direct search method, though precise, is time-consuming. In order to reduce computational effort, the control and sizing can be decoupled into two phases. In the first phase, annual simulations of the partial storage system along with MPC are performed. An electrical load profile from this first phase is then used as an input to a second phase for sizing the PV system. The second phase determines the optimal PV size according to the following optimization problem.

$$
\begin{aligned}
\min_{n \in Z} \quad & C^i_{PV} n + P_w \Big(\sum_{i=1}^{N_y} E(i) P_g(i) + \sum_{j=1}^{N_m} max(D(i)^j P_g(i)^j, 0) + C^m_{PV} n \Big) \\
\text{s.t.} \quad & P_g(i) = P_l(i) - P_s(i) \\
& \sum_{i=1}^{N_y} E(i) P_g(i) \geq 0 \\
& P_s(i) = n P_{si}(i) \\
& n \geq 0
\end{aligned}
\tag{4.1}
$$

where n is the number of PV panels (Model KC200GT for this study), C^i_{PV} is the installed cost per PV panel (1.88 \$/W installed cost for this study), C^m_{PV} is the maintenance fee per PV panel (assuming 18 \$/kW per year for maintenance), N_y is the total number of hourly time intervals in one year, N_m is the number of months, e.g., 12 for a year, P_g is the net hourly average power purchased from grid (kW), P_l is the hourly average building electricity load (kW), P_s is the total hourly average PV power generation rate (kW), P_{si} is the single PV panel power (kW) and P_w is the present worth factor for ten years associated with currency inflation and discount.

In optimization problem 4.1, P_l, P_{si}, E, D and P_w are all inputs. The first constraint is an energy balance on power for the building. The second constraint is based on the net energy metering policy that has an annual true-up such that the annual cumulative energy cost should be greater than 0 which gives an upper bound for PV capacity. The third equation calculates the total hourly average PV power generation rate of n PV panels. The last constraint simply denotes a lower bound for the PV panel number.

In the optimization problem, P_l is unknown for a system coupled with ice storage for the reason that ice storage can reshape the building electrical load. Different control decisions provide different building load profiles because of load shifting. Ideally, the control and sizing should be processed simultaneously. The sequential optimization method eliminates this coupling and runs a single annual simulation for a partial storage system with MPC but without PV. The building load profile from this sim-

ulation is then used as an input to the optimization problem 4.1 as P_l. Due to the efficiency and robustness of convex optimization, the optimal PV panel number n could be computed rapidly in the CVX within Matlab.

Optimal PV sizing validation

A summary of the optimal PV panel numbers for utility rate plan A10, GS-2B and GS-R are listed in table 4.1. The optimal PV sizes determined by the direct search method serve as the baseline for evaluating the sequential optimization.

Table 4.1.
Optimal PV panel number validation

Utility rate plan	Optimal PV panel number (Coupling control and sizing)	Optimal PV panel number (Decoupling control and sizing)
A10	900	901
GS-2B	0	0
GS-R	795	795

For utility rate A10, the optimal PV panel number computed by sequential optimization is 901, which is almost the same as the direct search optimal number of 900. For both approaches, the optimal PV panel numbers result in an annual energy cost of 0. Thus, the TOU energy rate for utility rate A10 is high enough so that the best decision is to use as much PV panel as possible. The maximum PV panel number is determined by the second constraint in optimization problem 4.1. The optimal PV panel numbers for GS-2B computed by the two methods are both exactly 0 for the reason that GS-2B has a relatively low TOU energy cost rate such that the pay back period for installation of PV is longer than ten years. The utility rate GS-R has a much higher TOU energy cost rate than utility rate GS-2B such that the optimal size of PV is again to install as much as possible leading to an annual energy cost of 0.

For all three cases, the sequential optimization approach gives essentially the same result as the direct search method.

The accuracy of the optimal PV panel size determined by the sequential optimization approach depends on how close the operating cost computed through the sequential optimization (SO) approach is to the direct search (DS) approach for a given PV size.

For a utility rate, such as GS-R, only having a TOU energy cost without demand charge, excess PV with net metering can be fed into the grid with the same retail price such that the optimal energy cost control input trajectory is not influenced by whether PV is coupled to the system or not. Therefore, the operating cost calculated by DS and SO for a given PV size are the same. For the utility rates considered, adding the demand charge has a small effect on this result because the optimal energy cost is insensitive to the demand charge.

4.2.2 Analysis of utility rate influence on optimal PV size

As shown in subsection 4.2.1, the optimal PV size for the three utility rates considered is either the maximum PV size determined by the net metering annual true up policy or no PV. The decision is based on whether the TOU energy cost rate of a utility plan is high enough or not to make the investment of PV beneficial to customers. In optimization problem 4.1, if we take off the demand cost part in the objective function, then it is a linear programming problem whose optimal solution, i.e., optimal PV panel number, either resides in the upper bound determined by the second constraint or the lower bound determined by the last constraint. Hence the demand charge can be considered as a perturbation to the original linear programming problem.

In order to visualize the influence of demand charge, for simplicity, the utility rate A10 TOU-energy cost and demand charge were scaled to obtain new utility rate plans. Figure 4.9 shows optimal PV panel number computed by the sequential optimization

approach as a function of the scaling factors for TOU energy and demand cost. The left blue region represents the utility rate plans that are not economically beneficial for integration of PV and the right yellow region is where investors should use as much PV panels as possible. It is observed that between the maximum and minimum PV panel regions there is a transition region where the optimal PV panel number is between the upper bound and lower bound. When demand charge is scaled by 0 (the x-axis), the transition region disappears due to the nature of this linear programming problem. When the demand charge scaling factor increases, the demand charge, as a perturbation for the original LP problem, starts to influence the optimal PV size. With a larger demand charge rate, there is a greater cost saving potential such that even with a lower TOU energy cost rate, customers could still benefit from integrating PV into the system. Hence the transition region shifts leftward and becomes larger as the demand charge increases.

Overall, this transition region is quite narrow and steep which denotes the influence of demand charge rate on optimal PV size determination is small. The primary cost saving consideration for integration of PV comes from the TOU energy cost rate value. If the sequential optimization method computes an optimal PV size that resides in this transition region, then the optimal point also depends on demand charge and the accuracy of SO compared to DS might start to deteriorate.

4.3 Optimal battery and photovoltaic size determination

Optimal sizing in terms of life cycle costs should be carried out in combination with optimal control. In the design stage, both demand and energy costs can be minimized to obtain a theoretical optimal solution using perfect knowledge of ambient conditions

and building loads. The optimization problem for sizing battery and photovoltaics is formulated as follows:

$$
\begin{aligned}
\min_{n\in Z, C_b\in R, P_b(i)\in R} \quad & C^i_{PV} n + C^i_{ba} C_b + P_w\Big(\sum_{i=1}^{N_y} E(i) P_g(i) \Delta T + \\
& \sum_{j=1}^{N_m} max(D(i)^j P_g(i)^j, 0) + C^m_{PV} n + C^m_{ba} C_b\Big) \\
\text{s.t.} \quad & P_g(i) = P_l(i) + P_b(i) - P_s(i) \\
& x_b(0) = x_{b,ini} \\
& x_b(i+1) = x_b(i) + \Delta T \frac{P_b(i)}{C_b} \\
& -C_r C_b \le P_b(i) \le C_r C_b \\
& x_{b,l} \le x_b(i) \le x_{b,u} \\
& \sum_{i=1}^{N_y} E(i) P_g(i) \Delta T \ge 0 \\
& P_s(i) = n P_{si}(i) \\
& n \ge 0
\end{aligned}
\tag{4.2}
$$

The optimization variables are n, C_b and $P_b(i)$ which are the number of PV panels, battery energy storage capacity (kWh) and hourly battery charging and discharging rates (kW). In the objective function, C^i_{ba} is the battery installed cost per unit of energy storage capacity ($/kWh) and C^m_{ba} is the battery maintenance cost($/kWh per year). C_r is the battery C-rate which in this study is 0.5. P_w is the net present factor for a ten-year analysis. The first constraint is the building electrical energy balance with a definition that battery charging is positive and discharging is negative. The initial state of charge, i.e., $x_{b,ini}$, is taken to be 0.25. The third constraint represents the battery dynamics. For the purpose of simplicity in the optimal sizing phase, the battery power rate lower and upper bounds are only determined by its C-rate, i.e., 0.5 in this study. In addition, battery state of charge is restricted between 0.25 and 0.95 to prevent over depletion and charge. The objective function is the sum of a linear term and a max function, so it is convex [29]. Within the constraints,

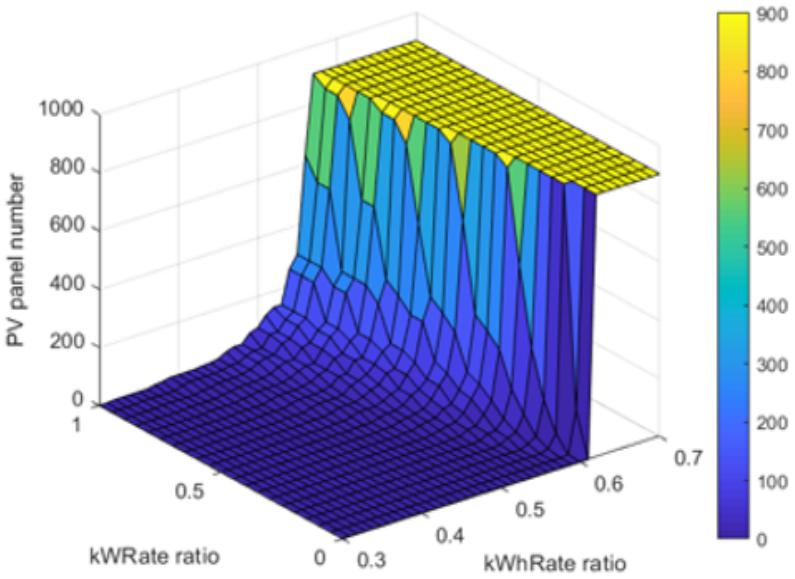

(a) Optimal PV panel number graph

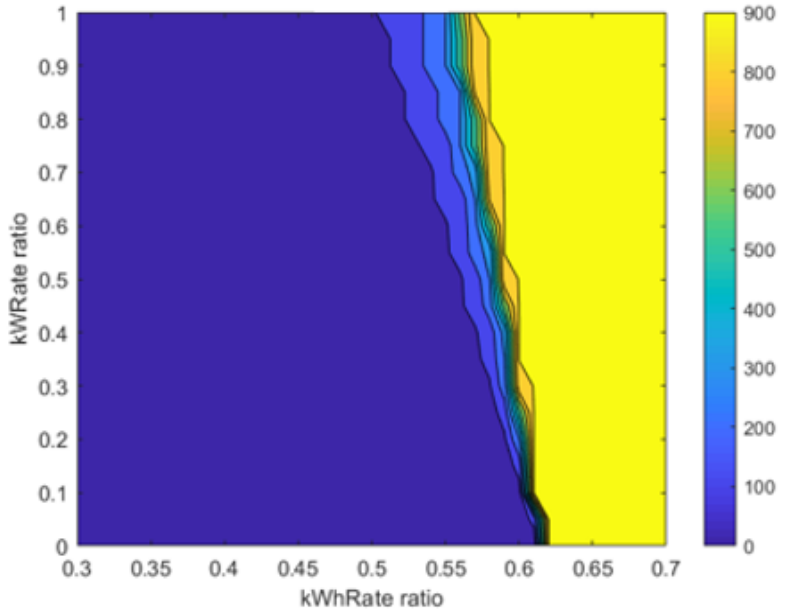

(b) Optimal PV panel number contour

Fig. 4.9. Variation of optimal PV size

note that the x_b dynamic equation is bi-linear which is not convex but all other

constraints are convex. Hence numerically, this optimization problem is solved as a convex optimization problem by varying P_b each time using CVX in Matlab.

Figure 4.10 shows optimal system life cycle cost and optimal PV panel number for utility rate A10 determined by varying battery capacities. Subfigure 4.10(a) shows that with the current installed costs (909 $/kWh), lithium-ion batteries are not economic for integration into the system. This is a natural result for a net energy metering policy where the extra self-generated energy can be directly sold back to the grid at the same retail price. In other policies, where the sell-back price is much lower than the purchase price, then the economic benefit of integrating batteries would be better. Subfigure 4.10(b) shows variation of optimal PV panel number with battery capacity. The scale is quite small and the optimal PV size has a small dependence on battery capacity.

Sensitivity of optimal battery size to installed costs

Even though the current installed cost for lithium-ion batteries is not favorable for integration, it is expected that the price will drop in the future. Figure 4.11 shows ten-year life cycle cost variation versus battery capacities for three installed costs of batteries of 909 $/kWh, 500 $/kWh and 200 $/kWh. Solid lines and dash lines represent ten-year life cycle costs and relative life cycle cost savings compared with the baseline that doesn't incorporate batteries and PV arrays, respectively. For the two lower battery costs, there is an optimal battery capacity of 85 kWh for 500 $/kWh with a 2.2 % life-cycle cost savings, and 150 kWh for 200 $/kWh with a 7.3 % life-cycle cost savings. Both cases illustrate a promising cost saving potential when the initial cost of battery drops with technology development in the future.

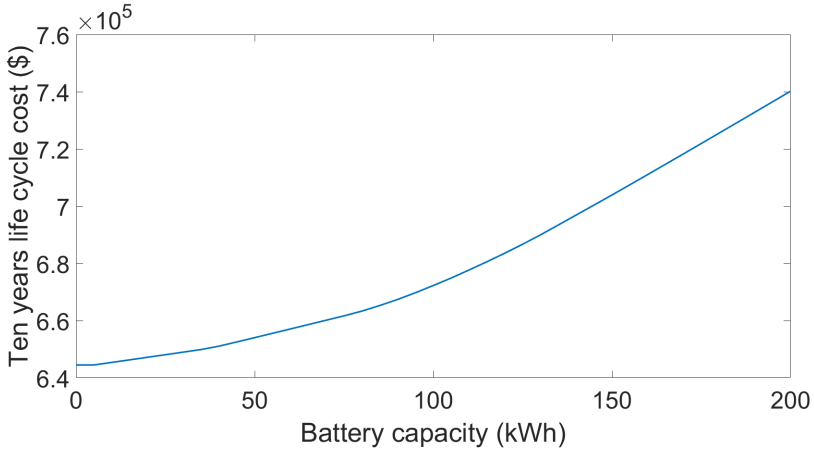

(a) Ten years life cycle cost

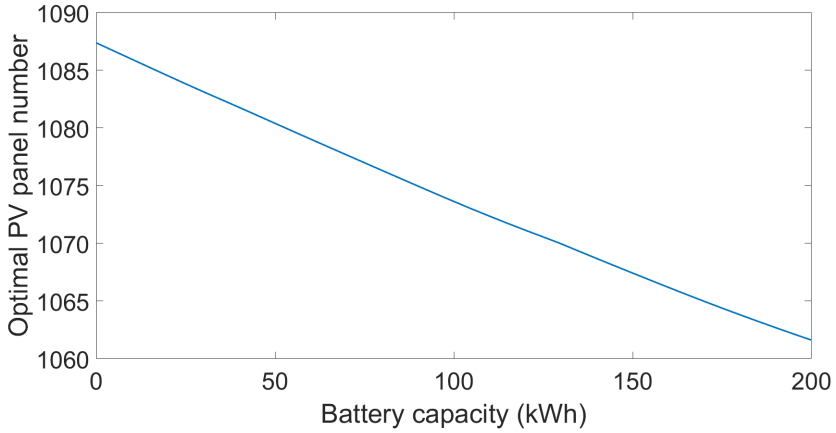

(b) Optimal PV panel number

Fig. 4.10. Variation of system optimal life cycle cost and PV size versus battery capacity for utility rate plan A10

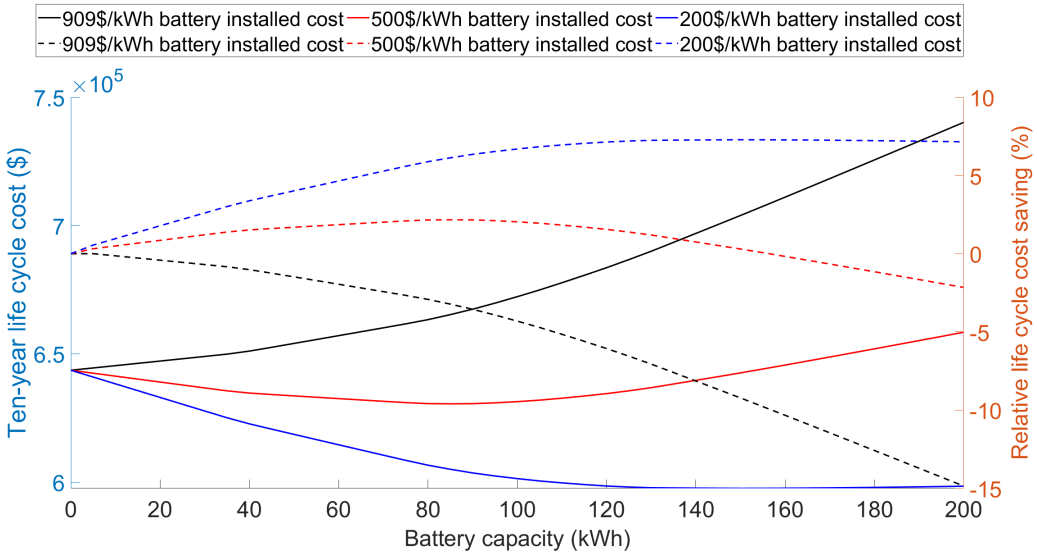

Fig. 4.11. Variation of system optimal life cycle cost versus battery capacity under different battery installed costs

5. ECONOMIC ANALYSIS OF PV SYSTEM COUPLED WITH ICE STORAGE OR BATTERIES

This chapter presents the results of the case study for Riverside, California that applies the proceeding models, model predictive control algorithm, and optimal component sizing approaches for the three representative utility rate plans (A10, GS-2B and GS-R), a net energy metering renewable energy policy, and the assumed system installed and maintenance costs. The ten-year life cycle economic performance of the PV system coupled either with ice storage or batteries were evaluated.

5.1 Comparison of optimal life cycle cost

System component optimal size selection

Table 5.1 summarizes the system component optimal sizing result for the case study described in previous chapters in terms of the life cycle cost.

For the central cooling system coupled with ice storage, the optimal ice storage and PV sizes were determined in two stages. The ice storage optimal size was taken to be a partial storage point since the life cycle cost sensitivities in this region are quite low for all three utility rate plans. The PV size was then computed from the optimization problem 4.1. Since utility rate A10 and GS-R have a high TOU-energy rate, the optimal PV size is the maximum PV size. On the contrary, utility rate GS-2B has a much lower TOU-energy rate such that not integrating PV is optimal in view of optimal life cycle cost.

For the central cooling system coupled with lithium-ion batteries, the current installed cost is too high for integration in a commercial building scale under a net energy metering policy and no battery is the best decision in terms of life cycle cost

Table 5.1.
System component optimal size selection

Central cooling system coupled with PV and ice storage			
	A10	GS-2B	GS-R
Chiller	45 ton	45 ton	45 ton
Ice storage	312 ton-hour	312 ton-hour	312 ton-hour
Photovoltaics	180 kW	0 kW	159 kW
Central cooling system coupled with PV and batteries			
	A10	GS-2B	GS-R
Chiller	75 ton	75 ton	75 ton
Battery	0 kWh	0 kWh	0 kWh
Photovoltaics	218 kW	0 kW	223 kW

for all three utility rate plans. Without thermal storage, the chiller size is determined by the design day building cooling load and a 75-ton chiller was selected for all three cases. It can be observed that the PV size without storage follows the same behavior when coupled with ice storage but with a larger size needed to achieve annual net-zero electrical costs.

Optimal life cycle cost

Life-cycle cost results for the different systems are summarized in figure 5.1. The baseline is a conventional HVAC system with a 75-ton chiller to meet the building cooling load and no PV or ice storage. The second bar in the figure is the life cycle cost for a central cooling system coupled with ice storage. The last two represent the optimal life cycle cost results for a central cooling system integrated with solar energy and either coupled with ice storage or not. The cases that consider integration of batteries with or without PV are not shown here since the optimal battery size is 0.

For two utility rate plans (A10 and GS-R), the system coupled with solar energy and thermal storage significantly reduces life cycle costs giving up to 35.6 % savings (see figure 5.3) for utility rate plan A10. For plan GS-2B, the TOU energy cost rate is too low and the optimal PV size is 0 leading to identical life-cycle costs for the ice storage only and combined PV and ice storage systems. It should be noted that the system coupled with batteries and PV has zero battery size as the optimum. However, lower battery costs in the future could change these economics.

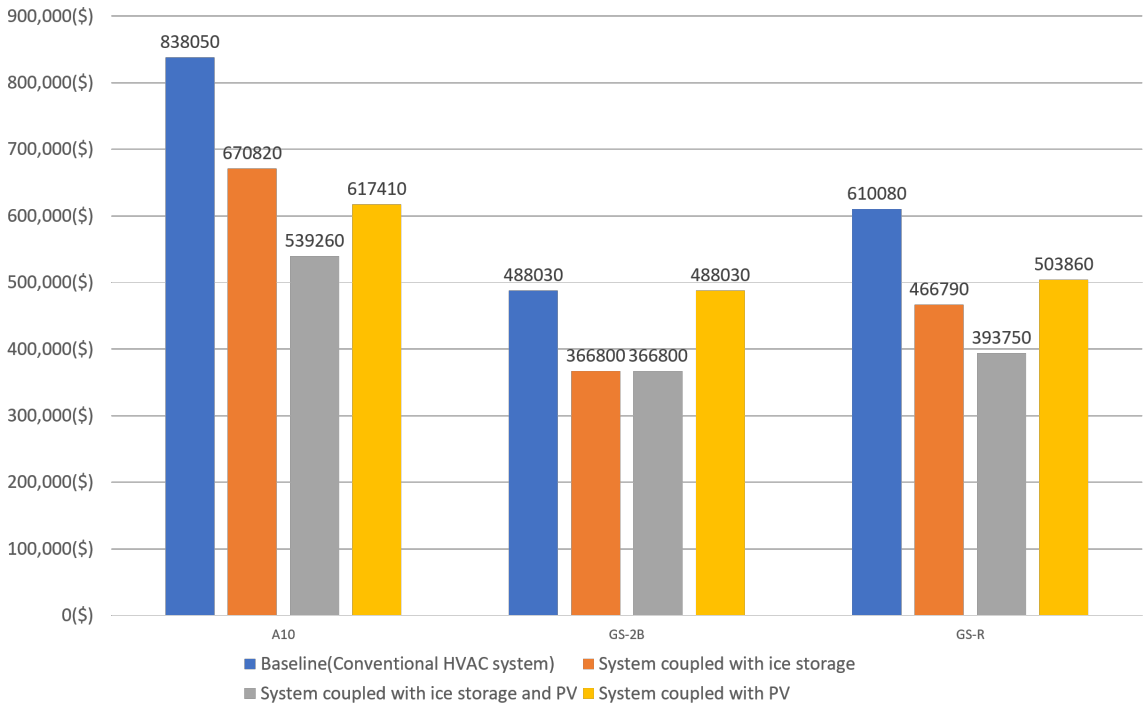

Fig. 5.1. Summary of life cycle costs

Figure 5.3 summarizes the installed costs, annual energy costs and demand charges for each utility rate plan. The installed cost difference between the baseline and the system coupled with ice storage is small, because the extra cost for storage is offset by reduced chiller costs. The installed costs for the system with PV are much higher. However, the energy costs with TOU rates are significantly reduced with integration of PV compared with the baseline and the system coupled with ice storage. Figure

5.2 shows the annual relative TOU-energy and demand cost savings in a comparison with the baseline for utility rate plan A10. The first and second sub-figures illustrate individual characteristics of ice storage and PV where ice storage performs better in reducing demand charges and PV is able to dramatically reduce energy costs. The last sub-figure illustrates the benefits of combining ice storage and PV in reducing both energy costs and demand charges. The last column bar in each subplot denotes the relative life cycle cost savings. These results demonstrate that the combination of ice storage and PV is the optimal choice for the case study considered with utility rate A10.

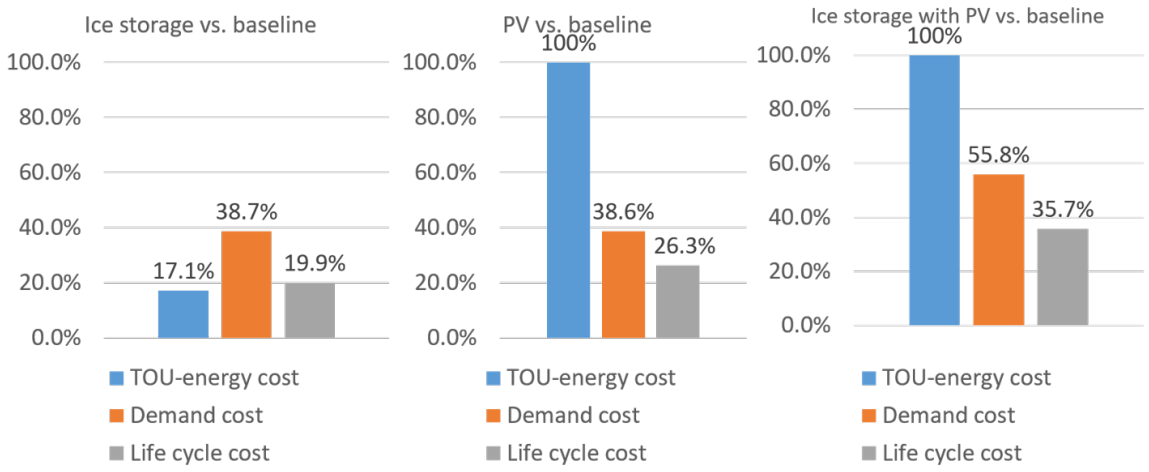

Fig. 5.2. Relative cost savings for utility rate plan A10

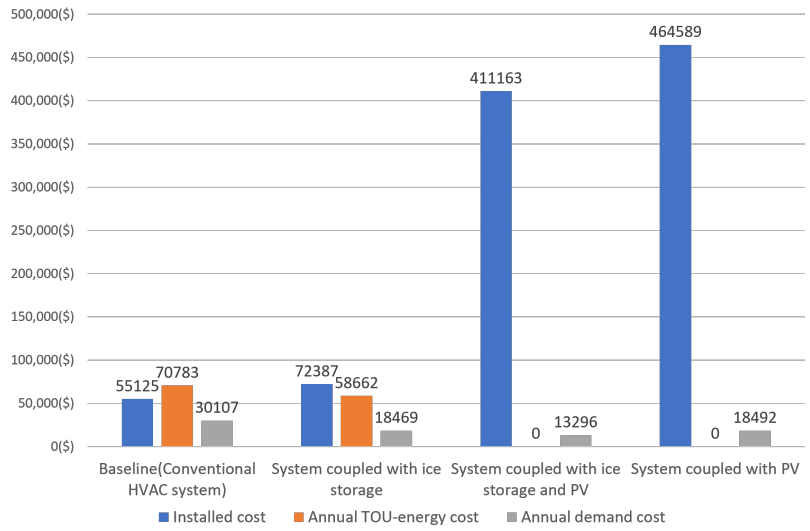

(a) Utility rate A10

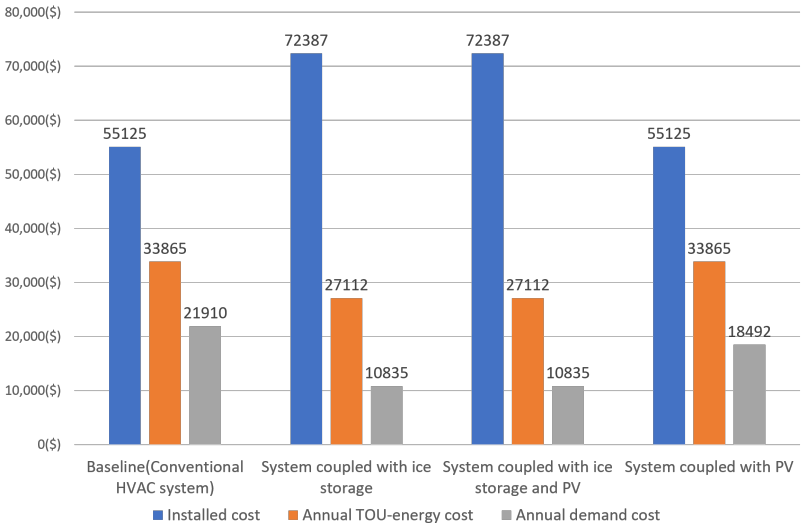

(b) Utility rate GS-2B

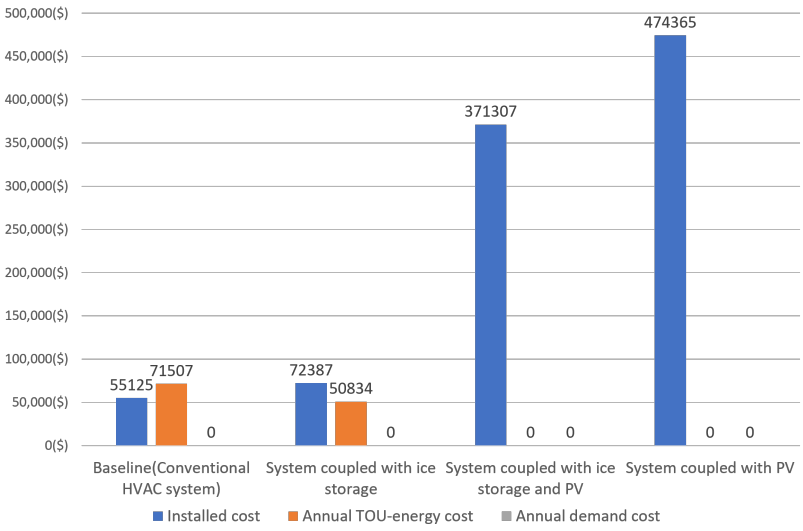

(c) Utility rate GS-R

Fig. 5.3. Summary of installed and operation costs

6. SUMMARY

6.1 Conclusions

This research focused on evaluation of the economic performance of a central cooling system with a photovoltaic array coupled with either thermal ice or battery storage. A case study for a medium size commercial building located in Riverside, California was performed. Three different representative utility rate plans were considered: TOU energy costs with an any time demand charge (A10), TOU energy costs with TOU demand charges (GS-2B), and only TOU energy costs (GS-R). A net energy metering policy was assumed throughout the case study which allows customers to sell back their self-generated power into the grid at the same retail price.

A simulation testbed was developed through empirical and semi-empirical approaches which contains an air-cooled chiller, ice storage tanks, pumps, building loads, batteries and PV array models. The chiller model determines maximum cooling capacity which serves as one of the constraints in an MPC problem and electrical power associated with a certain building load and operating conditions. A lumped ice storage model was implemented based on the concept of state of charge (SOC) and heat transfer effectiveness that accounts for energy efficiency penalties during charging and discharging processes. A detailed lithium-ion battery model from Matlab Simulink was used to obtain a simplified linear interpolation input-output model. A PV model was implemented based on a single diode with five unknown parameters that were obtained from a manufacturer's data sheet.

A fast numerical model predictive control algorithm was developed that could accomplish an annual simulation within a relatively short time. The near-optimal solution was facilitated by converting the original mixed-integer nonlinear programming (MINLP) problem into a nonlinear programming (NP) problem and by changing

the original combined energy cost and demand charge minimization problem into only minimizing short-term energy costs with a demand limit constraint. This NP problem was solved by backward dynamic programming in order to obtain a global optimal solution.

For a fair economic comparison, optimal system component sizing platforms were developed for each system. The system coupled with ice storage was sized by separating the central cooling plant and PV sizing into two sequential steps. Firstly, optimal life cycle cost graphs were generated by varying chiller and ice storage sizes for the three utility rate plans. For all three plans, it could be visualized that the minimum life cycle cost point is near the minimum chiller and ice storage sizes, which is the partial storage point. In addition, the sensitivity of life cycle cost to the sizing near the partial storage system point is pretty low such that the optimal chiller and ice storage size could be simply selected as partial storage. Next, a simplified method was developed to optimally size the PV capacity for the prescribed partial storage system through decoupling control and sizing into two phases. This sequential optimization approach was validated through comparison with a baseline approach that coupled control and sizing. The results showed the simplified approach works very well. For the case of the system coupled with batteries, a convex optimization approach was developed that couples control and sizing. The results showed that the lithium-ion battery installed costs were higher than a break even point in terms of ten-year life cycle costs such that the optimal battery capacity is zero.

In summary, the best system combination was found to be a partial storage system integrated with PV. Both ice and battery storage are able to reduce demand costs better than energy costs. On the contrary, PV is better at minimizing energy costs. The current installed costs for ice storage and PV are low enough to provide significant life-cycle savings over a ten-year analysis. However, the first cost of batteries is above a break even point. A sensitivity analysis of lithium-ion battery installed costs showed that cost savings could be achieved if installed costs fall below 500$/kWh. Batteries are much more flexible than ice storage in that they can shift both HVAC and non-

HVAC electrical loads. Therefore, with declining costs of batteries it is expected that it will be economically beneficial and feasible to include battery storage in commercial buildings in the future.

6.2 Future work

From the results, it could be observed that even though ice storage is better than battery storage at present in terms of overall life cycle economics, this system can only shift HVAC loads. Even after shifting all the HVAC load, the net power purchased from the grid is the difference between the non-HVAC electrical load and the solar power generation rate which could still have power spikes. In the future, it could be beneficial to utilize ice storage to shift HVAC loads, and batteries to shave the remaining power peak. Therefore, the current platform for optimal control and sizing could be extended to consider a combined system that contains ice storage, batteries and PV together. In addition, more case studies should be performed with different utility rate plans, multiple building types and climate zones.

REFERENCES

REFERENCES

[1] *Decision adopting successor to net energy metering tariff.* California Public Utilities Commission, 2016.

[2] D. Sera, R. Teodorescu, and P. Rodriguez, "Pv panel model based on datasheet values," in *2007 IEEE international symposium on industrial electronics*. IEEE, 2007, pp. 2392–2396.

[3] M. G. Villalva, J. R. Gazoli, and E. Ruppert Filho, "Comprehensive approach to modeling and simulation of photovoltaic arrays," *IEEE Transactions on power electronics*, vol. 24, no. 5, pp. 1198–1208, 2009.

[4] J. E. Braun, "A comparison of chiller-priority, storage-priority, and optimal control of an ice-storage system," *ASHRAE Trasaction*, vol. 98, pp. 893–902, 1992.

[5] K. H. Drees and J. E. Braun, "Development and evaluation of a rule-based control strategy for ice storage systems," *HVAC&R Research*, vol. 2, no. 4, pp. 312–334, 1996.

[6] J. Candanedo, V. Dehkordi, and M. Stylianou, "Model-based predictive control of an ice storage device in a building cooling system," *Applied Energy*, vol. 111, pp. 1032–1045, 2013.

[7] Y. Ma, A. Kelman, A. Daly, and F. Borrelli, "Predictive control for energy efficient buildings with thermal storage: Modeling, stimulation, and experiments," *IEEE control systems magazine*, vol. 32, no. 1, pp. 44–64, 2012.

[8] S. J. Cox, D. Kim, H. Cho, and P. Mago, "Real time optimal control of district cooling system with thermal energy storage using neural networks," *Applied energy*, vol. 238, pp. 466–480, 2019.

[9] K. J. Kircher and K. M. Zhang, "Model predictive control of thermal storage for demand response," in *2015 American Control Conference (ACC)*. IEEE, 2015, pp. 956–961.

[10] J. Braun *et al.*, "Supervisory control strategies and optimization," *ASHRAE Applications Handbook*, p. 64, 2015.

[11] Y. Lu, S. Wang, Y. Sun, and C. Yan, "Optimal scheduling of buildings with energy generation and thermal energy storage under dynamic electricity pricing using mixed-integer nonlinear programming," *Applied Energy*, vol. 147, pp. 49–58, 2015.

[12] J. Vetterli and M. Benz, "Cost-optimal design of an ice-storage cooling system using mixed-integer linear programming techniques under various electricity tariff schemes," *Energy and buildings*, vol. 49, pp. 226–234, 2012.

[13] J. West and J. E. Braun, "Modeling partial charging and discharging of area-constrained ice storage tanks," *HVAC&R Research*, vol. 5, no. 3, pp. 209–228, 1999.

[14] T. R. Ran Fu and R. Margolis, *2018 U.S. utility-scale photovoltaics-plus-energy storage system costs benchmark*. National renewable energy laboratory, 2018.

[15] D. F. Ran Fu and R. Margolis, *U.S. solar photovoltaic system cost benchmark: Q1 2018*. National renewable energy laboratory, 2018.

[16] D. susan schoenug, Ph, *Energy storage systems cost update*. Sandia national laboratories, 2011.

[17] X. Jin, A. Vora, V. Hoshing, T. Saha, G. Shaver, R. E. García, O. Wasynczuk, and S. Varigonda, "Physically-based reduced-order capacity loss model for graphite anodes in li-ion battery cells," *Journal of Power Sources*, vol. 342, pp. 750–761, 2017.

[18] A. Nottrott, J. Kleissl, and B. Washom, "Energy dispatch schedule optimization and cost benefit analysis for grid-connected, photovoltaic-battery storage systems," *Renewable Energy*, vol. 55, pp. 230–240, 2013.

[19] I. Ranaweera and O.-M. Midtgård, "Optimization of operational cost for a grid-supporting pv system with battery storage," *Renewable Energy*, vol. 88, pp. 262–272, 2016.

[20] J. Cai, X. Jin, and H. Zhang, "Economic model-based control of sustainable buildings with photovoltaic (pv) and battery systems considering battery degradation costs," in *2018 Annual American Control Conference (ACC)*. IEEE, 2018, pp. 5406–5411.

[21] J. Li and M. A. Danzer, "Optimal charge control strategies for stationary photovoltaic battery systems," *Journal of Power Sources*, vol. 258, pp. 365–373, 2014.

[22] X. Wang and M. Dennis, "Influencing factors on the energy saving performance of battery storage and phase change cold storage in a pv cooling system," *Energy and Buildings*, vol. 107, pp. 84–92, 2015.

[23] M. Saffari, A. de Gracia, C. Fernández, M. Belusko, D. Boer, and L. F. Cabeza, "Optimized demand side management (dsm) of peak electricity demand by coupling low temperature thermal energy storage (tes) and solar pv," *Applied energy*, vol. 211, pp. 604–616, 2018.

[24] U. D. of Energy. (1999) Commercial prototype buliding models. [Online]. Available: https://www.energycodes.gov/development/commercial/prototype models90.1

[25] Liu, *Prototype Building Models- Medium Office*. United States Department of Energy, 2016.

[26] R. Z. Kurt Roth and J. Brodrick, "Cool thermal energy storage," *American Society of Heating, Refrigerating and Air-Conditioning Engineers*, vol. 48, pp. 94–96, 2006.

[27] D. Kim, "Development, evaluation and demonstration of model predictive control for an ice storage," 2018.

[28] D. P. Bertsekas, *Dynamic programming and optimal control (volume 1).* Athena scientific, 2017.

[29] S. Boyd and L. Vandenberghe, *Convex optimization.* Cambridge, 2004.